Molecular Therapy
Original Article

Tumor cell-secreted exosomal miR-22-3p inhibits transgelin and induces vascular abnormalization to promote tumor budding

Yaju Feng,[1,2,3,6] Lumeng Wang,[2,3,6] Ting Wang,[1] Ying Li,[1] Qingqing Xun,[1,4] Renya Zhang,[1] Lin Liu,[5] Lei Li,[1] Wei Wang,[1] Yixuan Tian,[2,3] Lili Yang,[1] Xiao Zhi,[1] Bijiao Zhou,[2,3] Xin Chen,[2,3] Tao Sun,[2,3] and Yanrong Liu[1]

[1]Department of Pathology, Affiliated Hospital of Jining Medical University, Jining Medical University, Jining 272029, Shandong, China; [2]State Key Laboratory of Medicinal Chemical Biology and College of Pharmacy, Nankai University, Tianjin 300350, China; [3]Tianjin Key Laboratory of Early Druggability Evaluation of Innovative Drugs and Tianjin Key Laboratory of Molecular Drug Research, Tianjin International Joint Academy of Biomedicine, Tianjin 300457, China; [4]School of Clinical Medicine, Jining Medical University, Jining 272029, Shangdong, China; [5]Health Management Center, Affiliated Hospital of Jining Medical University, Jining Medical University, Jining 272029, Shandong, China

Tumor budding (TB) is considered a histomorphological marker of poor prognosis in patients with breast cancer (BC). Tumor vasculature is disordered and unstable in BC, which causes restricted drug delivery, hypoxia, and tumor metastasis. Traditional anti-angiogenic treatments cause extreme hypoxia, increased invasion, metastasis, and drug resistance due to blood vessel rarefaction or regression. Therefore, the application of anti-angiogenic strategies for vascular normalization in tumors is crucial to improve therapeutic efficacy in BC. In the present study, we found that transgelin (TAGLN) promoted the normalization of tumor vessels by regulating the structure and function of endothelial cells, and knockout of TAGLN in tumor-bearing mice resulted in tumor vessel abnormalization, an increase in epithelial-mesenchymal transition characteristics of tumor cells, and promotion of TB. Moreover, BC cells secrete exosomal miR-22-3p that mediates tumor vessel abnormalization by inhibiting TAGLN. We demonstrated for the first time that TAGLN plays an essential role in tumor vessel normalization, and thus it impairs TB and metastasis. Additionally, the findings of this study indicate that exosomal miR-22-3p is a potential therapeutic target for BC.

INTRODUCTION

Breast cancer (BC) is the second leading cause of cancer-related deaths in women.[1] Although current antitumor treatments improve the 5-year survival rate in patients with BC, the recurrence and metastasis of BC after surgical resection of the primary tumor are the major causes of death in patients undergoing BC treatment. Detailed mechanisms of metastasis in BC are complicated. Thus, knowledge of the exact mechanism may help in developing new diagnostic markers and treatment targets.

Tumor budding (TB) is a histopathological finding identified by the observation of a single cell or a cluster of fewer than five cells in the invasive front of a tumor.[2,3] TB can be observed in invasive tumors and is a prognostic factor for colorectal cancer,[4] lung cancer,[5,6] head and neck squamous carcinoma,[7] pancreas squamous carcinoma,[8] and esophageal squamous carcinoma.[9] Additionally, extensive TB is directly related to lymphatic vessel invasion, large tumor size, and poor prognosis in BC.[10–12] TB can be observed during the invasive stages of cancer because of the detachment of a few tumor cells from the main tumor body.[13,14] The level of E-cadherin (a critical molecule for intercellular adhesion of epithelial cells) is low in tumor buds of cancer.[15–18] Loss of E-cadherin localization in the membrane can serve as a marker for epithelial-mesenchymal transition (EMT).[19] In EMT, epithelial cells lose intercellular adhesion and gain migration and invasion capabilities, which are the characteristic of mesenchymal cells.[20] Consequently, TB is "EMT-like";[21] however, the precise TB mechanism in the context of BC remains unknown.

Growth and metastasis of solid tumors highly depend on tumor angiogenesis, and thus many angiogenesis inhibitors have been developed for cancer treatment in recent decades.[22] Traditionally, anti-angiogenic treatments mainly focus on suppressing angiogenesis and destroying the existing tumor vasculature to starve tumor cells. However, the clinical outcomes of these treatments are still not satisfactory because these treatments usually cause severe hypoxia in the tumor because of blood vessel rarefaction or regression, eventually enhancing drug resistance and peripheral tissue invasion as well as aggravating metastasis. In normal tissues, pro-angiogenesis and

Received 15 April 2020; accepted 4 February 2021;
https://doi.org/10.1016/j.ymthe.2021.02.009.

[6]These authors contributed equally

Correspondence: Tao Sun, State Key Laboratory of Medicinal Chemical Biology and College of Pharmacy, Nankai University, No. 38 Tongyan Road, Jinnan District, Tianjin 300350, China.
E-mail: sunrockmia@hotmail.com
Correspondence: Yanrong Liu, Department of Pathology, Affiliated Hospital of Jining Medical University, Jining Medical University, No. 89 Guhuai Road, Jining 272029, Shandong, China.
E-mail: liuyanrong1984@163.com

anti-angiogenesis are in equilibrium. However, this balance is disrupted in tumor tissues. Tumor vascular vessels exhibit structural abnormalities, such as increased MVD and distorted, swollen, and cystic vascular morphology.[23] Moreover, pericytes exhibit abnormal morphology, which inhibits their function, leading to lost or absence of connectivity. The basement membrane of the blood vessels is incomplete with uneven thickness.[24] Dysfunctional tumor vasculature limits the effective perfusion of oxygen and drug delivery.[25] The strategy for tumor vascular normalization was proposed to enhance tumor perfusion and drug delivery by improving vessel maturity, blood perfusion, and oxygenation and decreasing the interstitial fluid pressure.[26] However, the exact mechanism underlying tumor vascular normalization requires further clarification

Transgelin (TAGLN), first identified in 1987, is a 22-kDa protein with unknown functions, and it has also been named as mouse p27, WS3-10, and SM22-α.[27] It is a type of actin-binding protein that participates in cytoskeletal remodeling and modulates the balance between polymeric filamentous (F)-actin and monomeric (G)-actin. TAGLN can directly interact with F-actin, boost the crosslinking activity, and facilitate actin filaments in bundles.[28] Its expression is related to angiogenesis, and it plays an essential role in vasculogenic mimicry in BC, which is a vascular formation mechanism used by aggressive tumor cells.[29]

Exosomes are endosome-derived membrane vesicles, with diameters ranging from 30 to 120 nm; they can be secreted by both normal and malignant tumor cells.[30] Tumor-derived exosomes play a key role in intercellular communications by selectively delivering their cargoes (membrane or inner proteins, DNAs, and microRNAs [miRNAs]) into distant target cells.[31] miRNAs released by cancer cells can be transferred to the surrounding endothelial cells (ECs) through exosomes, which is crucial to the execution of biological activities of ECs.[32]

In this study, we performed a clinical case analysis and cell culture experiments and used a tumor-bearing xenograft mouse model to confirm that TAGLN stimulates the normalization of tumor vessels by regulating the structure and function of ECs. Knockout of the TAGLN gene resulted in tumor vessel abnormalization, increasing in the EMT characteristics of tumor cells, and promotion of TB in BC. Moreover, BC cell-derived exosomes mediated tumor vessel abnormalization through miR-22-3p, which was shown to inhibit TAGLN. Salvianolic acid A (SAA), a small molecule that targets TAGLN,[33] was found to promote tumor vessel normalization in the BC tumor-bearing mouse model.

In the present study, we primarily demonstrated the role of TAGLN in normalization of tumor blood vessels, which impaired TB and metastasis of BC cells. These findings may provide considerable clarity in developing BC-targeted treatments in the future.

RESULTS

BC tissues with high budding number have increased abnormal tumor vessels

The relationship between TB and the clinicopathological characteristics of human BC tissues was analyzed, and TB was found to be associated with large tumor size, high lymph node metastasis status, clinical stage and pathological grade of the cancer, and low survival rate (Figure 1A). TB manifests the EMT phenotype and exhibits high laminin 5γ2 expression.[34] Thus, in the present study, we explored the expression of EMT markers in TB-positive tissues. E-cadherin expression was downregulated, whereas those of vimentin and laminin 5γ2 expression were upregulated in TB cells, which confirmed the EMT characteristics of TB cells (Figure 1B). To further determine the relationship between TB and tumor angiogenesis, we analyzed the relationship of TB with microvessel density (MVD) and microvascular structural entropy (MSE). We found that tumor tissues with higher TB exhibited increased MVD and MSE (Figure 1C). Immunofluorescence (IF) analysis of CD34 was then performed to determine the relationship between vascular density, vascular morphology, and TB. High budding tissues resulted in increased vascular density, and the vessels were irregular and tortuous with increased vascular sprouting (Figure 1D). Furthermore, we found that high budding BC tissues exhibited the increased abnormalization of tumor vessels with decreased coverage of pericytes and basement membrane, and adhesion ability of ECs, which were presented as reduced co-localization of CD34 with PDGFRβ, collagen type IV, and VE-cadherin, respectively (Figure 1E).

Decreased endothelial TAGLN expression leads to vascular abnormalization of tumor

A co-culture model was used to determine the exact mechanism of tumor vessel abnormalization; human umbilical vein ECs (HUVECs) and MCF-7/MM-231 BC cells were seeded in the lower and upper compartment of the transwell assay, respectively. Increased migration ability of HUVECs was observed after co-culturing them with BC cells (Figure 2A). Their tube formation ability was also enhanced, as revealed by the number, vessel length, and branching junctions of tubes (Figure 2B). Spheroid-based angiogenesis assays demonstrated more spouting and tube extension in HUVECs after co-culturing them with BC cells (Figure 2C). Decreased expression of VE-cadherin in co-cultured HUVECs implied fewer connections between ECs (Figure 2D), thereby possibly increasing the permeability (Figure 2E). Fewer cell junctions, irregular and flattened shapes, and decreased cell pseudopodia were observed under a scanning electron microscope (SEM) (Figure 2F). Moreover, the cytoskeleton was destroyed in the co-culture model (Figure 2G). These results indicated that HUVECs co-cultured with BC cells exhibit vascular abnormalization. TAGLN, a cytoskeleton-related protein, directly interacts with F-actin to stimulate the crosslinking activity of F-actin and facilitates the assembly of actin filaments during bundle formation.[35] TAGLN expression is high in ECs,[36] and it participates in new blood vessel formation of tumor cells.[29] Hence, we speculated that TAGLN was involved in vascular abnormalization in the co-culture model. TAGLN expression was determined by western blot and IF assays in HUVECs or HUVECs co-cultured with BC cells. TAGLN expression was found to decrease in HUVECs co-cultured with BC cells (Figures 2H and 2I). In co-cultured HUVECs, the expression of F-actin decreased, whereas that of G-actin increased (Figure 2J), thereby confirming the possible regulatory effects of TAGLN.

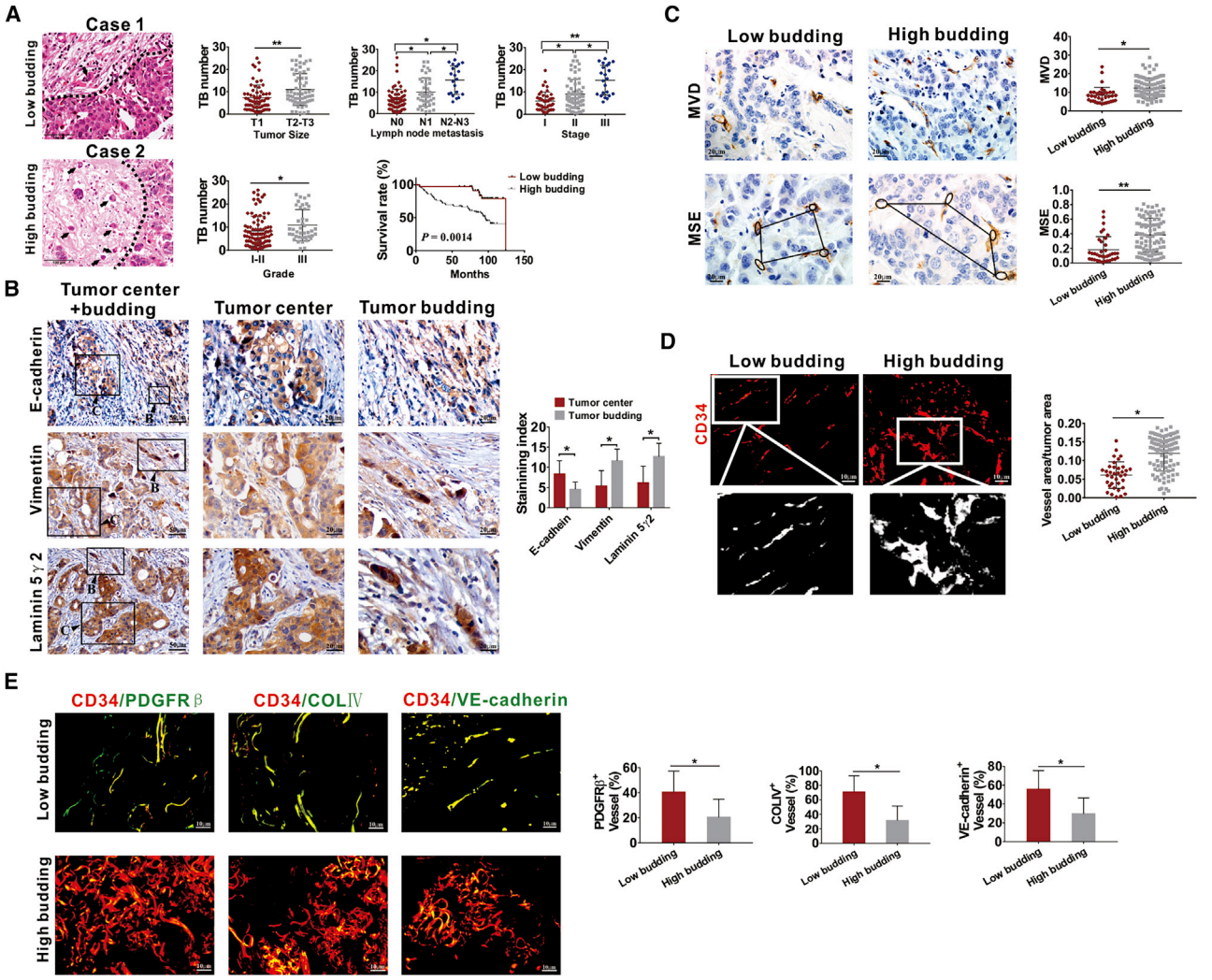

Figure 1. Breast cancer (BC) tissues with high TB exhibit increased abnormalization of tumor vessels

(A) Representative images of TB in human BC tissues and relationship of TB with clinicopathological parameters and survival of patients with BC. The dotted line indicates the boundary between tumor mass and budding areas. The arrow points to the budding cells. (B) Expression of EMT markers in TB-positive BC tissues detected by IHC. "B" represents TB, and "C" represents the tumor center. (C) Quantification of MVD and MSE in BC tissues detected by CD34 IHC staining. MSE was estimated according to the relationship between the area of neighboring microvessels and the distance between them. (D) Representative images of $CD34^+$ blood vessels and quantification of vessel area in BC tissues stained by IF assays. (E) The coverage of $PDGFR\beta^+$ pericytes, coverage of type IV collagen$^+$ basement membrane, along with distribution of VE-cadherin within $CD34^+$ vessels in BC tissues with low or high TB. The coverage of $PDGFR\beta^+$ pericytes, type IV collagen, and VE-cadherin is shown in the manner of the percent of length lying along the $CD34^+$ vessel. *$p < 0.05$, **$p < 0.01$.

Furthermore, we examined different extents of vascular abnormalization and expression of TAGLN in endothelial vessels in the tumor area and paracarcinoma tissues by examining the co-localization of CD34, PDGFRβ, collagen type IV, VE-cadherin, and TAGLN. Normal tissues adjacent to the tumor region displayed more normal vessels and higher TAGLN expression in endothelial vessels than in the BC tumor regions (Figure 3A). Then, we determined the relationship between the numbers of TAGLN-positive blood vessels and the clinicopathological characteristics of patients with BC. BC patients at an advanced stage displayed a lower number of TAGLN-positive blood vessels (Figure 3B). The reduced number of TAGLN-positive blood vessels was also related to large tumor size, high lymph node metastasis status, and pathological grade of the cancer (Figure 3C). We then analyzed the expression of TAGLN in tumor vessels and found decreased expression of TAGLN in the tumor vessels of human BC tissues with high TB (Figure 3D). Moreover, the reduced number of TAGLN positively stained blood vessels was also related to the low survival rate in patients with BC (Figure 3E). To further confirm the findings, we used the Gene Expression Profiling Interactive Analysis (GEPIA) database to analyze the expression of TAGLN in BC samples. TAGLN in 1,085 BC tissues was found to be significantly decreased compared with normal tissues ($p < 0.01$) (Figure S1A).

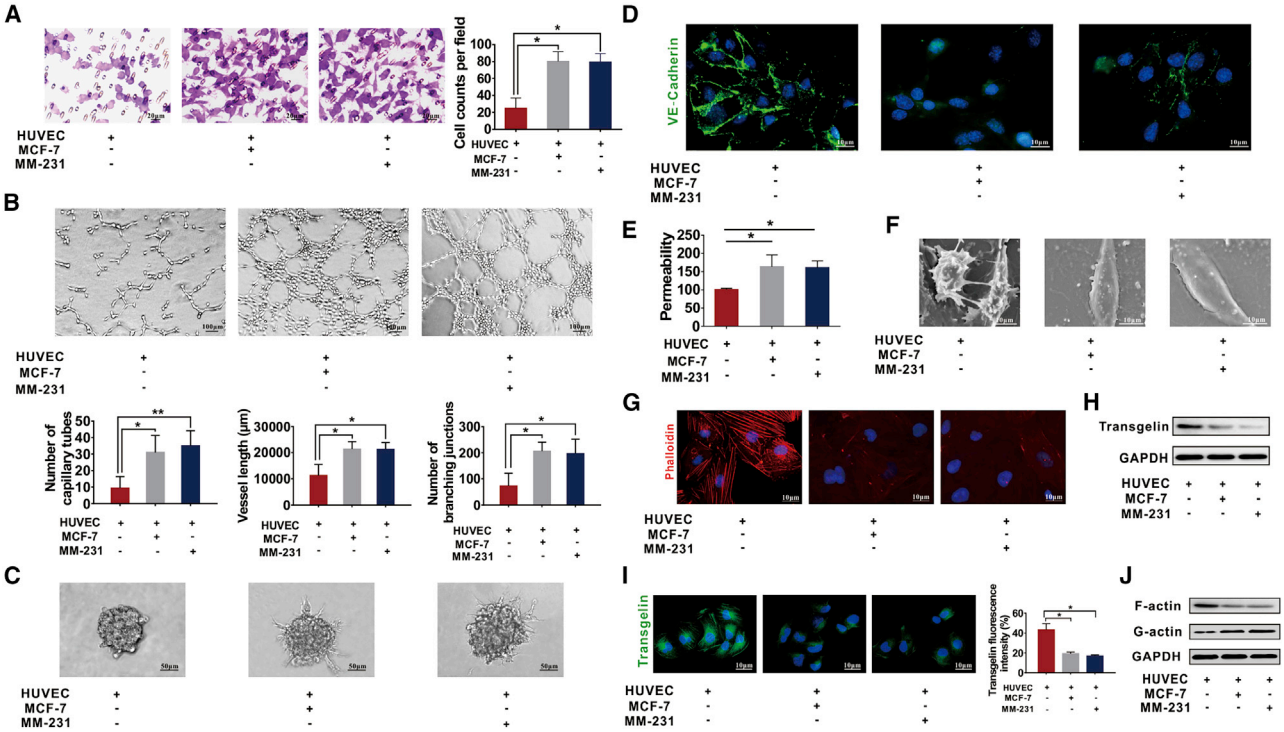

Figure 2. HUVECs co-cultured with MCF or MM-231 cells exhibit abnormal vascularization and decreased transgelin (TAGLN) expression

(A) Transwell assays were performed to measure the migration ability of HUVECs co-cultured with MCF-7 or MM-231 cells. (B) HUVECs co-cultured with MCF-7 or MM-231 cells displayed a high number of capillary tubes, vessel length, and branching junctions in the tube formation assay. (C) Co-cultured HUVECs had increased spheroid sprouting, tube extension, and branching in the spheroid-based angiogenesis assay. (D) HUVECs co-cultured with MM-231 or MCF-7 cells had reduced expression of VE-cadherin, as shown in the IF assays. (E) Increased permeability was found in HUVECs co-cultured with MCF-7 or MM-231 cells examined a by rhodamine-dextran permeability assay. (F) Fewer cell junctions and increased cell pseudopodia were observed under a scanning electron microscope in HUVECs co-cultured with MCF-7 or MM-231 cells. (G) MCF-7/HUVEC or MM-231/HUVEC co-culture has an impaired cytoskeleton in the cytoskeleton staining assay. (H) Decreased TAGLN expression was observed in HUVECs co-cultured with BC cells in western blot assays. (I) Decreased TAGLN expression was observed in HUVECs co-cultured with BC cells in IF assays. (J) F-actin expression was decreased and G-actin expression was increased in HUVECs co-cultured with BC cells as detected by western blot assays. Results were repeated three times in independent experiments. *$p < 0.05$, **$p < 0.01$.

Further statistical analysis based on Human Protein Atlas (HPA) databases showed that patients with high expression of TAGLN have better prognosis than do other patients (Figure S1B).

To further verify the effects of TAGLN on vascular normalization *in vitro*, we transfected the normal HUVECs with TAGLN small interfering RNA (siTAGLN) and overexpressed TAGLN in HUVECs co-cultured with BC cells (Figure 4A). The migration, tube extension, sprouting ability, and vessel length of HUVECs was decreased when TAGLN was overexpressed in the co-cultured HUVECs. However, these effects were increased in TAGLN-knockdown HUVECs (Figures 4B–4D). Cytoskeletal formation and F-actin expression were increased, whereas the G-actin expression was decreased when TAGLN was overexpressed in the co-cultured HUVECs. However, the knockdown of TAGLN in HUVECs resulted in decreased cytoskeletal formation and F-actin expression and increased G-actin expression (Figures 4E and 4F). Moreover, the expression of VE-cadherin was increased (Figure 4G), whereas the permeability of co-cultured HUVECs was decreased with TAGLN overexpression (Figure 4H). These results indicated that TAGLN exhibits a regulatory effect on the normalization of cultured vascular ECs.

Xenografts transplanted in TAGLN knockout mice exhibit increased invasive potential

To further investigate the role of TAGLN on angiogenesis and the invasive potential of tumors *in vivo*, we established an E0771 BC tumor-bearing mouse model (wild-type [WT] or Tagln$^{-/-}$ mice). SAA, the primary bioactive ingredient extracted from *Salvia miltiorrhiza* and extensively used in the treatment of cardiovascular diseases, can specifically stabilize the TAGLN-actin complex, and thus it regulates actin cytoskeletal remodeling, facilitates F-actin bundling, and enhances coronary blood flow and contractility.[31] In this study, we speculated whether SAA could regulate the normalization of tumor blood vessels by stabilizing the TAGLN-actin complex and eventually exerting its anti-tumor effects. The transplanted tumor in Tagln$^{-/-}$ mice grew significantly faster than in the WT mice. Tumor volumes of SAA-treated WT mice were also lower than those of the untreated WT mice. However, these differences were not statistically significant

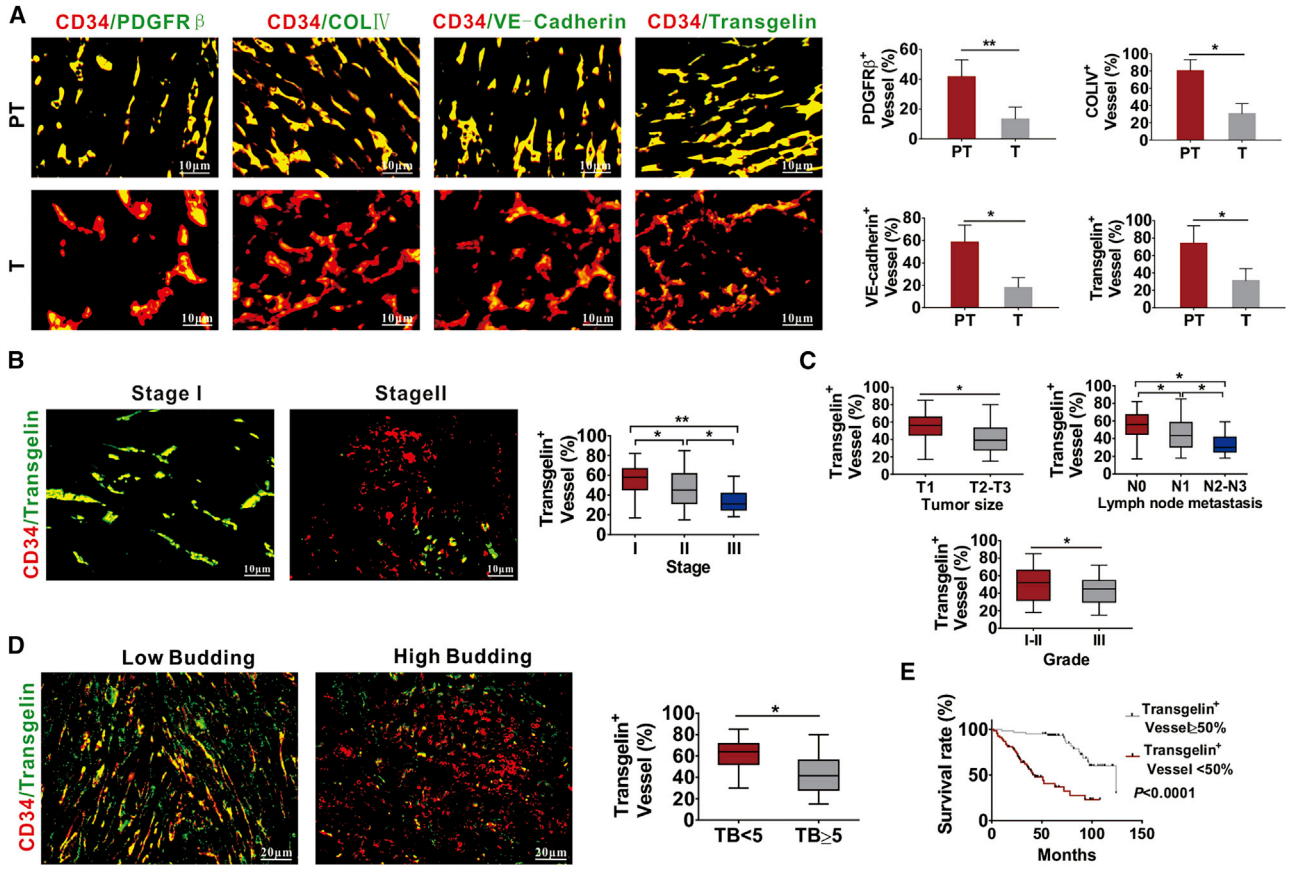

Figure 3. Expression of TAGLN in tumor vessels is related to TB and prognosis of human BC

(A) Tumor vessels in paracancerous tissue had increased PDGFRβ$^+$ pericyte coverage, collagen type IV$^+$ basement membrane coverage, distribution of VE-cadherin, and higher TAGLN coverage in endothelial vessels than in the tumor regions. CD34$^+$ tumor blood vessels were stained for PDGFRβ, collagen type IV$^+$, VE-cadherin, and TAGLN. PT, paracancerous tissue; T, tumor region. (B) BC tissues with high clinical stage had fewer numbers of TAGLN positively stained blood vessels. (C) The reduced number of TAGLN positively stained blood vessels was related to the large tumor size, high lymph node status, and pathological grade. (D) BC tissues with a high number of TB displayed fewer TAGLN positively stained blood vessels. (E) The reduced number of TAGLN positively stained blood vessels was related to the low survival rate in patients with BC. *p < 0.05, **p < 0.01.

(Figure 5A). The survival rate of tumor-bearing Tagln$^{-/-}$ mice was shorter than that of WT mice (p = 0.0368), and SAA significantly increased overall survival in the WT mice (p = 0.0447, Figure 5A). We also found that SAA treatment has no therapeutic effect on transplanted tumor in the Tagln$^{-/-}$ mice (Figure 5A). We further examined the lung metastasis foci (Figure 5B) and invasion areas (Figure S2A) in the transplanted tumor tissues. Tagln$^{-/-}$ mice displayed larger metastastic size (Figure 5B) and invasion areas (Figure S2A) than did WT mice. Moreover, SAA exhibited an inhibitory effect on WT mice but not on Tagln$^{-/-}$ mice (Figures 5B and S2A). Thereafter, alterations in vascular structure and functions in the transplanted tumor tissue were determined on the basis of hypoxia status, dextran leakage, vascular perfusion, and normalization of tumor vessels. Transplanted tumors in Tagln$^{-/-}$ mice exhibited increased blood vascular density, hypoxia areas, and dextran leakage but less vascular perfusion (Figure 5C). PDGFRβ$^+$ pericyte coverage, collagen type IV$^+$ basement membrane coverage, distribution of endothelial junctional molecules such as VE-cadherin, and expression and localization of TAGLN in the CD34-labeled endothelial vascular vessels were also determined. The transplanted tumor tissues in Tagln$^{-/-}$ mice exhibited decreased PDGFRβ$^+$ pericyte coverage, collagen type IV$^+$ basement membrane coverage, and VE-cadherin distribution on tumor vessels. TAGLN expression and localization in the CD34-labeled endothelial vascular vessels of Tagln$^{-/-}$ tumors were also decreased (Figure 5D). The results also suggested that SAA improved the vascular perfusion and normalization of vessels in tumor tissues of WT mice, but no such effects were observed in the tumor-bearing Tagln$^{-/-}$ mice. Afterward, the expression of EMT markers was determined, which suggested the upregulation of vimentin and laminin 5γ2 (mesenchymal markers) and downregulation of E-cadherin (epithelial marker) (Figure S2B). Based on the effects of TAGLN on improvement in the disorganized tumor vessel function, we speculated whether the TAGLN-targeting drug, SAA, could enhance the drug delivery efficiency when combined with the

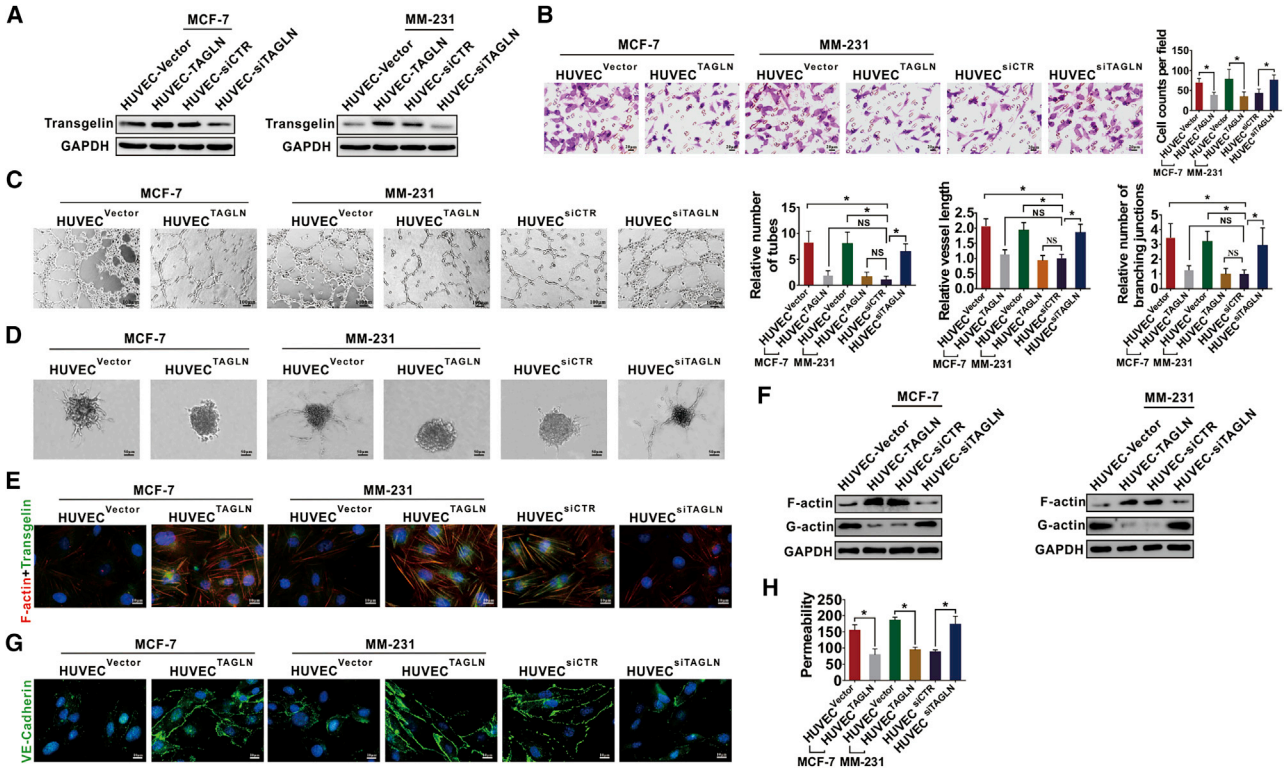

Figure 4. TAGLN expression in the endothelial cells regulates tumor vascular normalization *in vitro*

(A) HUVECs were transfected with siTAGLN, and the co-cultured HUVECs were overexpressed with TAGLN. The transfection efficiency was verified by western blot assays. (B) The transwell migration assays showed the migration ability of HUVECs or co-cultured HUVECs with different expression of TAGLN. (C) The tube formation assays showed the relative number, vessel length, and branching junctions of the capillary tubes formed by HUVECs cultured on Matrigel to the HUVEC siCTR group. (D) The spheroid-based angiogenesis assay showed the sprouting and tube extension of HUVECs, with different expression levels of TAGLN. (E) Cytoskeletal formation and expression of TAGLN in HUVECs determined in IF assays. (F) Expressions of F-actin and G-actin in HUVECs with different expression levels of TAGLN were determined by western blot assays. (G) Expression of VE-cadherin of HUVECs with different expression levels of TAGLN was examined in IF assays. (H) Permeability of HUVECs with different expression levels of TAGLN was examined by a rhodamine-dextran permeability assay. Results were repeated 3 times in independent experiments. *p < 0.05.

chemotherapeutic drug cisplatin (DDP). The transplanted tumor grew slower in the combination therapy group compared with the single drug group. However, the difference did not attain statistical significance (Figure 5E). The SAA + DPP combination prolonged the survival time of the tumor-bearing mice more significantly than did DDP alone ($p = 0.0478$, Figure 5E). The combination of SAA + DPP more significantly suppressed lung metastasis than did individual treatments (Figure 5F). The combination therapy group demonstrated increased necrotic area and decreased expression of HIF-1α in the transplanted tumor tissues compared with the single-drug group (Figures 5G and S2C). Thus, the results confirmed that the combined effect of SAA and DDP is superior.

Tumor-derived exosomes inhibit TAGLN in HUVECs

Considering the regulatory effects of exosomes on tumor angiogenesis,[37,38] we speculated that the effects of TAGLN on tumor vessel normalization were related to those of exosomes. We isolated exosomes from cultured BC cells *in vitro* and assessed the regulatory effects of tumor-derived exosomes on TAGLN expression in HUVECs. BC cell-derived exosomes were found to be 30–100 nm in size, as determined through transmission electron microscopic (TEM) analysis (Figure 6A), and they stained positive for CD63, TSG101, and Hsp70 expressions (Figure 6B). PKH26-labeled exosomes were found to enter HUVECs (Figure 6C). Effects of exosomes on migration and tube formation ability were determined in the co-culture model. MCF-7- or MM-231-derived exosomes promoted the abnormal vascularization of HUVECs, which was confirmed by their increased migration ability (Figure 6D), number of tubes, branching junctions, and vessel length (Figure 6E). Moreover, BC cell-derived exosomes promoted spouting and tube extension of HUVECs (Figure 6F). These promotion effects in co-cultured HUVECs were abolished when GW4869 was added (Figures 6D–6F). The expression of VE-cadherin was decreased, whereas the permeability was increased when HUVECs were treated with exosomes, and the aforementioned effects were inhibited when GW4869 was added (Figures 6G and 6H). We also determined whether tumor cell-derived exosomes could regulate TAGLN expression. TAGLN expression was decreased (Figure 6I), the cytoskeleton was destroyed (Figure S3A), F-actin expression was downregulated, and G-actin expression was upregulated (Figure S3B) after the treatment of HUVECs with BC cell-derived

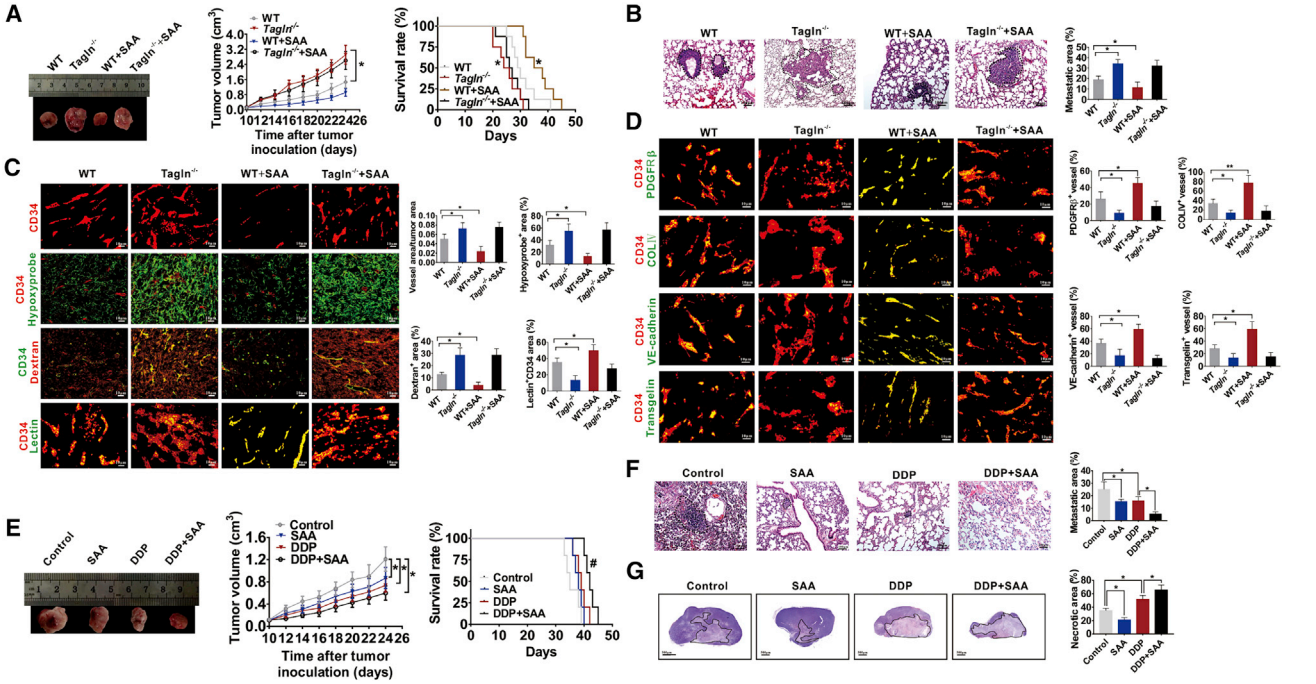

Figure 5. TAGLN knockout in mice induces tumor progression and tumor vessel abnormalization, and SAA enhanced DPP delivery to tumors

(A) Growth of E0771 tumors and survival curves of E0771 tumor-bearing WT or Tagln$^{-/-}$ mice with or without SAA treatment. *p < 0.05 versus WT. (B) Representative images of pulmonary metastasis areas in WT or Tagln$^{-/-}$ mice. The dotted line demarcates the metastasis areas in the lung tissue. (C) Representative images and quantification for CD34^{+} vascular areas, Hypoxyprobe^{+} regions in tumors, dextran leakage, as well as lectin perfusion from tumor vessels. (D) Representative images for the coverage of PDGFRβ^{+} pericytes, coverage of type IV collagen^{+} basement membrane, along with the distribution of VE-cadherin and TAGLN within the CD34-labeled endothelial blood vessels. (E) The tumor growth curve and survival rate curve of the transplanted E0771 tumor with different drug treatment. (F) Representative images and quantification of the lung metastasis areas of the tumor-bearing mice. The dotted line demarcates the metastasis areas in the lung tissue. (G) Images and comparison of the necrotic areas of the transplanted tumors. Solid lines demarcate the necrosis areas. *p < 0.05, **p < 0.01, #p < 0.05, compared to the DDP group.

exosomes; these effects were inhibited in the co-cultured HUVECs when GW4869 was added. Thus, the results support our hypotheses.

BC cells transfer miR-22-3p to HUVECs through exosomes to suppress TAGLN expression

miRNAs play an essential role in angiogenesis and can be transferred intercellularly via exosomes.[39,40] We determined whether the regulatory effects of exosomes on tumor angiogenesis are due to the effects of exosomal miRNAs. The miRBase (http://www.mirbase.org/) and TargetScan (http://www.targetscan.org/) databases were used to predict the possible TAGLN-targeting miRNAs, which were later intersected with miRNAs derived from BC exosomes. As shown in Figure 7A, miR-22-3p was identified. Thereafter, the binding sites between miR-22-3p and TAGLN were examined through bioinformatics analysis, which suggested that miR-22-3p interacts with the 3′ UTR of TAGLN via a 7-bp region (Figure 7B). Thereafter, a luciferase assay was performed to confirm the interaction between miR-22-3p and the 3′ UTR of TAGLN. Consequently, miR-22-3p mimic-transfected cells exhibited markedly downregulated luciferase activity. Moreover, luciferase activity in the mutant group was not inhibited after transfection with miR-22-3p mimics, which indicated that TAGLN was the direct target of miR-22-3p (Figure 7C). Next, we found that miR-22-3p was significantly increased in HUVECs treated with exosomes isolated from BC cells (MCF-7 and MM-231 cells) compared with that in the PBS-treated HUVECs (Figure 7D). MM-231 BC cells were then infected with the empty lentivirus control vector, or lentivirus to overexpress or knock down miR-22-3b, and the exosomes were isolated. Increased miR-22-3p expression was found in the HUVECs treated with exosomes overexpressing miR-22-3p (Figure 7E). Furthermore, we found that when miR-22-3p overexpressing exosomes (miR-22-3p OE Exos) were added to the culture medium of HUVECs, the expression of TAGLN in HUVECs was decreased (Figure 7E). We then transfected MM-231 BC cells seeded on the upper chamber of the transwell assays with fluorescent Cy3-labeled miR-22-3p and assessed Cy3 levels in HUVECs (seeded in the lower chamber of the transwell assays) by using fluorescence microscopy after co-culturing for 3 days (Figure 7F). Red fluorescence (Cy3 expression) in HUVECs indicated the transfer of Cy3-miR-22-3p from MM-231 cells of the upper transwell chamber to HUVECs of the lower transwell chamber (Figure 7F). Therefore, miRNAs released from BC cells could be transferred to HUVECs. To confirm whether exosomal miR-22-3p induces abnormal angiogenesis by targeting TAGLN, HUVECs were treated with MM-231 exosomes, MM-231 exosomes with miR-22-3p knocked down, and MM-231 exosomes

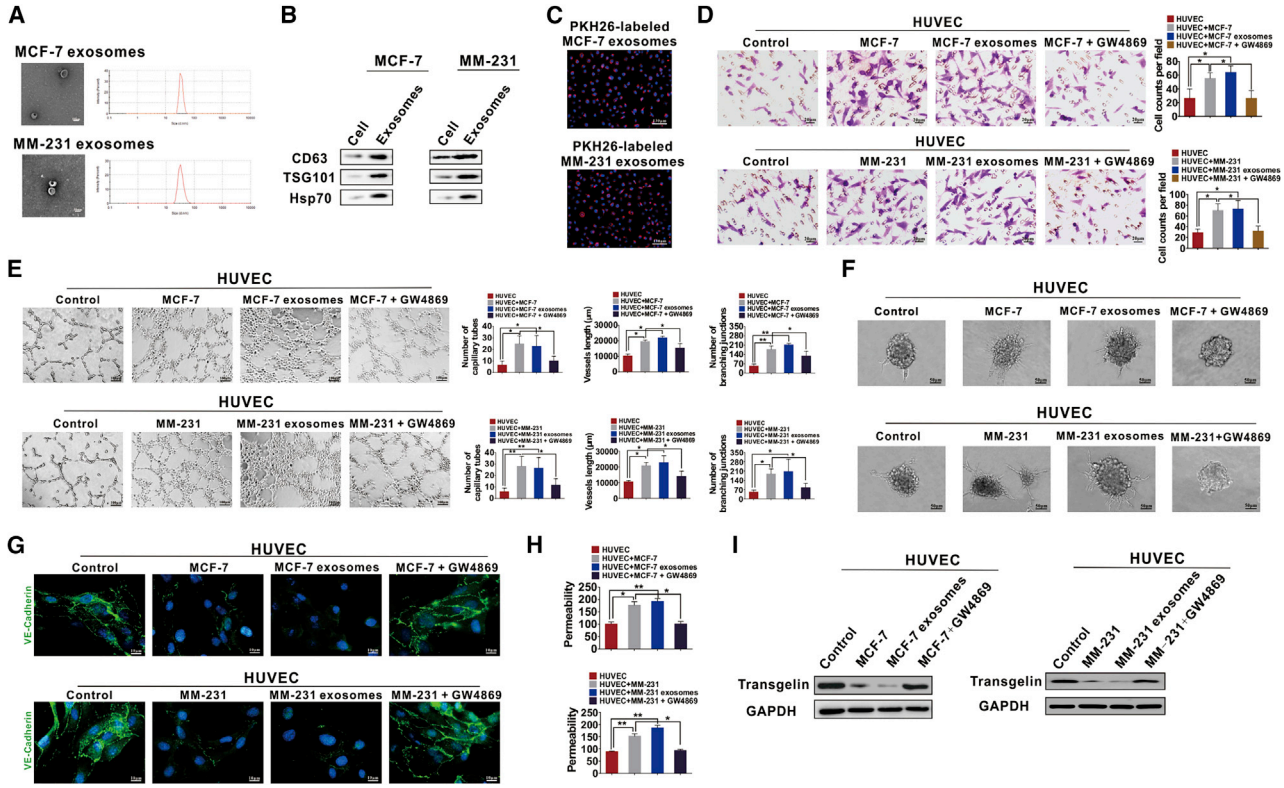

Figure 6. Tumor-derived exosomes induced the abnormal tube formation of HUVECs and downregulated the expression of TAGLN

(A) A TEM and a particle size analyzer were used to analyze the isolated exosomes. (B) TSG101 (the marker specific to exosome), together with HSP70 and CD63 (protein markers associated with extracellular vesicle), was detected through western blotting. (C) MCF-7 or MM-231 cell-derived exosomes were conjugated with PKH26 before adding into the HUVEC medium. (D) Tumor exosomes increased the migration of HUVECs. The increased migration ability of co-cultured HUVECs can be suppressed by GW4869, which inhibits exosome generation. (E) Effects of exosomes on tube formation abilities of HUVECs cultured on Matrigel. The ability of tube formation in HUVECs was enhanced by coincubation with BC exosomes. (F) Spheroid-based human endothelial cell sprouting was determined by the hanging drop method. BC exosomes increased spheroid sprouting and branching of HUVECs. (G) Expression of VE-cadherin was examined by IF assays. Weakened VE-cadherin staining at cell-cell contact sites can be found in co-cultured HUVECs or HUVECs treated with BC exosomes. The aforementioned effects were inhibited when GW4869 was added. (H) The permeability of HUVEC monolayers was determined by dextran rhodamine clearance. (I) Expression levels of TAGLN were determined by western blot analysis. Results were repeated three times in independent experiments. *$p < 0.05$, **$p < 0.01$.

after overexpressing TAGLN in HUVECs. We found that HUVECs treated with exosomes exhibit decreased TAGLN expression (Figure 7G). When the HUVECs were treated with miR-22-3p-knockdown exosomes, the expression of TAGLN was restored, which suggests that the regulatory effects of exosomes on the expression of TAGLN are dependent on miR-22-3p levels (Figure 7G). HUVECs treated with MM-231 exosomes displayed decreased F-actin expression (Figure 7H) and disrupted cytoskeletons (Figure 7I); the effects were reversed when miR-22-3p was knocked down, which suggests that the regulatory effects of exosomes are dependent on miR-22-3p levels (Figures 7H and 7I). Overexpression of TAGLN in HUVECs reversed the effects of exosomes, suggesting that the regulation of TAGLN expression may be the possible mechanism involved in BC exosome-mediated effects (Figures 7H and 7I). We found that MM-231 exosomes also increased the migration (Figure 7J), tube formation (Figure 7K), and sprouting ability (Figure 7L) of HUVECs, and these effects can be reversed by knocking down miR-22-3p. Additionally, exosomes from MM-231 cells decreased the VE-cadherin expression (Figure 7M) and increased the permeability of HUVECs (Figure 7N), and these effects were reversed by miR-22-3p knockdown. Overexpression of TAGLN in HUVECs reversed the aforementioned effects of exosomes derived from BC cells (Figures 7J–7N).

Exosomal miR-22-3p promotes tumor progression and angiogenesis *in vivo* by targeting TAGLN

Subsequently, the function of exosomal miR-22-3p in regulating abnormal blood vessel and tumor development was assessed via tumor-bearing WT or Tagln$^{-/-}$ mice. Tumor volume and survival of the tumor-bearing mice were recorded. Exosomes extracted from E0771 cells transfected with lentivirus empty control or miR-22-3p-knockdown lentivirus were injected into the mice via the caudal vein. Compared with the control group, the tumor volume was increased in the exosomes and miR-22-3p OE group (Figure 8A). Additionally, exosomes and miR-22-3p treatment significantly

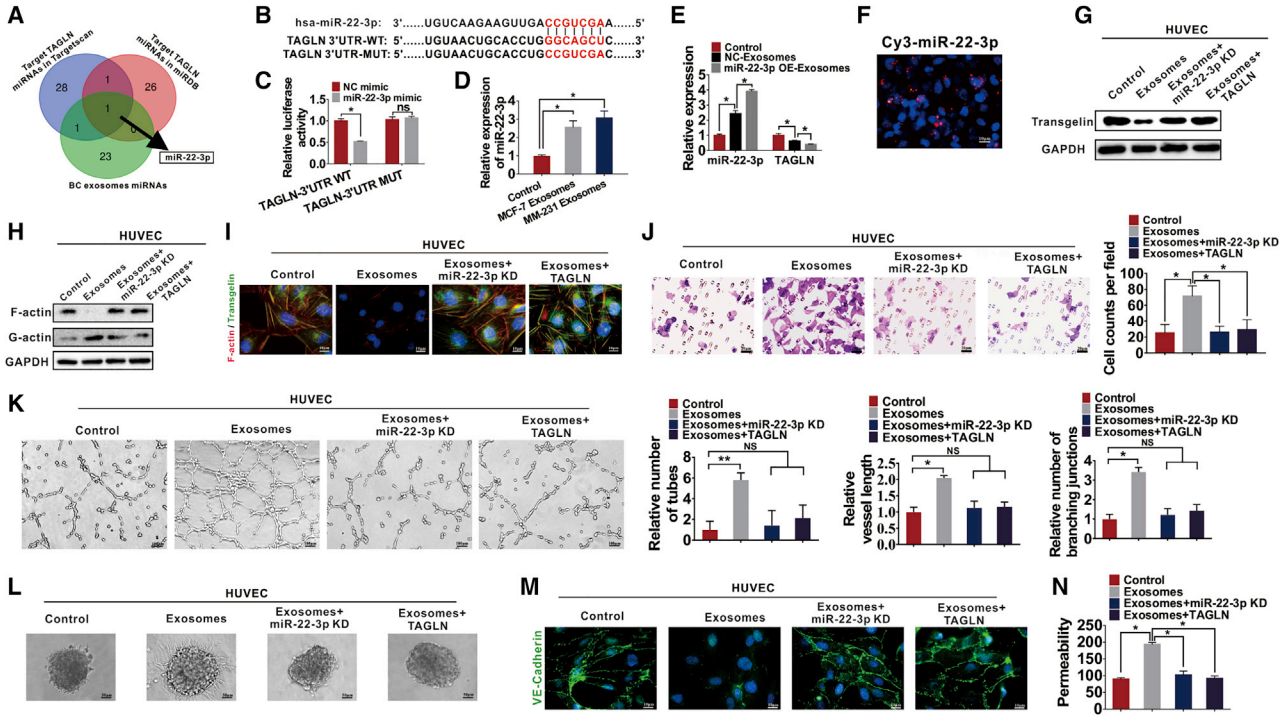

Figure 7. BC cells transfer miR-22-3p through exosomes to suppress TAGLN expression and regulate the angiogenesis ability of HUVECs

(A) Potential miRNAs targeting TAGLN were predicted using the TargetScan and miRBase databases and intersected with the BC exosomal miRNAs. miR-22-3p was set as the intersection. (B) Predicted binding sites of miR-22-3p within the 3′ UTR of TAGLN. (C) Relative luciferase activities of MM-231 cells subjected to co-transfection of miR-22-3p mimics with firefly luciferase reporter plasmid that contained WT or mutant TAGLN 3′ UTR. (D) Relative miR-22-3p expression in HUVECs cultured by diverse exosomes detected through quantitative real-time PCR. (E) miR-22-3p or TAGLN expression in HUVECs following NC-Exos or miR-22-3p-Exos treatment detected through quantitative real-time PCR. (F) Cy3-labeled miR-22-3p mimic-transfected MCF-7 and MM-231 cells were subjected to HUVECs co-culture detected through transwell assays. (G) TAGLN levels in HUVECs under diverse treatments detected by western blotting. (H) F-actin and G-actin levels after treatment with different exosomes were detected in HUVECs through western blotting. (I) IF staining was performed to analyze the F-actin cytoskeleton and TAGLN in HUVECs treated with various exosomes. (J) Migration ability of HUVECs was measured by transwell assays. (K) Tube formation assays were used to determine the relative tube number, vessel length, and number of branching junctions of vessels to control. (L) The hanging drop method was performed to determine the spheroid-based human endothelial cell sprouting. (M) Expression of VE-cadherin in HUVECs was determined by IF assays. (N) The permeability of HUVEC monolayers was determined by dextran rhodamine clearance. Results were repeated three times in independent experiments. *$p < 0.05$, **$p < 0.01$.

decreased the overall survival time of WT mice (the p value was 0.0045 and 0.0018, respectively, Figure 8B). These effects were reversed after exosome treatment when miR-22-3p expression was inhibited (Figures 8A and 8B). Exosomes and miR-22-3p treatments also increased invasion and lung metastasis in WT tumors (Figures S4A and S4B). Then, we examined the effects of exosomal miR-22-3p on tumor progression in $Tagln^{-/-}$ mice. Consistently, exosomes and miR-22-3p treatment exhibited no effect on the growth, invasion, and metastasis of tumor and survival of the tumor-bearing $Tagln^{-/-}$ mice (Figures 8A, 8B, S4A, and S4B). Subsequently, the transplanted tumors were collected, and the hypoxia statuses, vessel perfusion, and vascular abnormalization were analyzed. Exosomes and miR-22-3p treatment dramatically increased the vessel density, hypoxic area, and dextran leakage, and markedly decreased vascular perfusion in WT mice, but the treatment was found to have no effect on $Tagln^{-/-}$ tumors (Figure 8C). Exosomes and miR-22-3p treatment also increased the vessel density and decreased the PDGFR β, COLIV, and VE-cadherin coverage in tumor vessels of WT tumors, whereas these effects were not observed in $Tagln^{-/-}$ tumors (Figure 8D). Expressions of vimentin and laminin 5γ2 were increased, whereas that of E-cadherin was decreased in WT tumors treated with exosomes or miR-22-3p, whereas no such effect was observed in *TAGLN*$^{-/-}$ tumors (Figure S4C).

DISCUSSION

Tumor blood vessels exhibit poor or inefficient perfusion because they are irregular and structurally disordered, which leads to extreme hypoxia, increased tumor invasion, distant metastasis, and refractoriness to chemotherapy.[24] Traditionally, anti-angiogenic drugs used for "vessel pruning" may exacerbate hypoxia in tumors and deteriorate malignant tumor conditions.[41] Normalization of tumor vessels was shown to improve clinical responses in diverse subsets of patients with cancer.[42] However, the precise mechanism underlying blood vessel abnormalization remains to be elucidated.

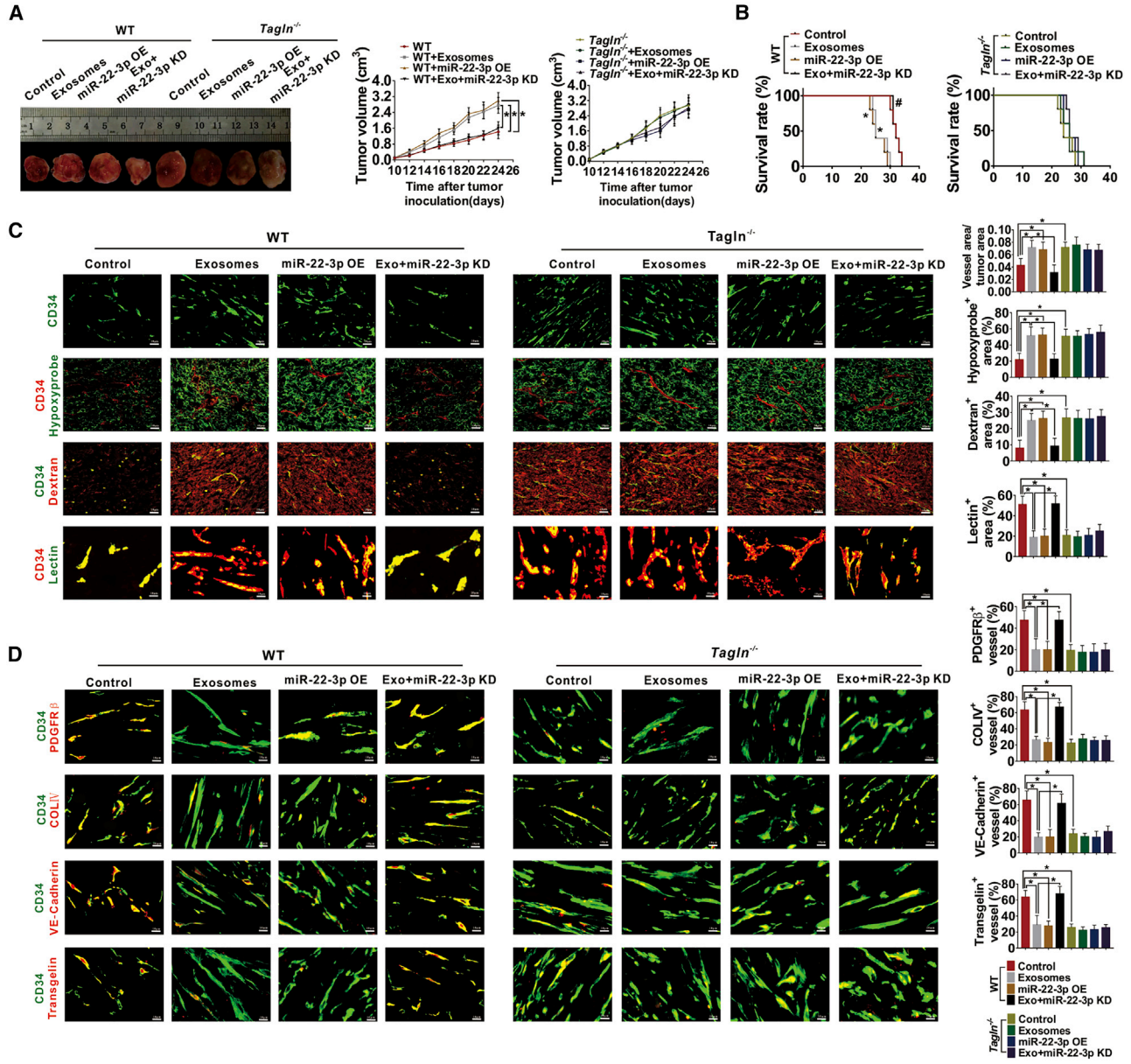

Figure 8. Exosomal miR-22-3p enhanced tumor progression and angiogenesis of WT tumors but did not affect *Tagln*$^{-/-}$ tumors

(A) The panel on the left shows typical images for E0771 xenografts obtained in WT or *Tagln*$^{-/-}$ mice with different treatments, whereas that on the right presents the growth curve of xenograft volume. *$p < 0.05$. (B) The survival curve of E0771-bearing WT or *Tagln*$^{-/-}$ mice. *$p < 0.05$ versus WT; #$p < 0.05$ versus exosomes. (C) Representative images and quantification for vascular areas, Hypoxyprobe^{+} regions in WT or *Tagln*$^{-/-}$ tumors, lectin perfusion, and dextran leakage from tumor vessels of the transplanted tumors. (D) Coverage of PDGFRβ^{+} pericytes, coverage of type IV collagen^{+} basement membrane, and the distribution of VE-cadherin within CD34-labeled endothelial blood vessels in tumors harvested on day 24.

In this study, TAGLN, an actin-binding protein, was found to regulate the normalization of tumor vessels, increase tumor perfusion, and inhibit TB and metastasis. The association between TAGLN expression in tumor cells and cancer proliferation or invasion has been extensively studied; however, reports on the effect of TAGLN expression on tumor cells are conflicting. For instance, the TAGLN level was found to have decreased in BC and CRC,[43] but other studies have reported that the TAGLN level within tumor cells is positively correlated with stemness, invasion, and metastasis in hepatocellular carcinoma,[44] breast cancer,[45] and colorectal cancer.[46] Although several studies have addressed the role of tumor cell-derived TAGLN in tumorigenesis and progression, the role of endothelial TAGLN in tumor angiogenesis has not yet been clarified.

TAGLN overexpression has been reported to reduce the network formation, network stability, and migration of endothelial colony-forming cells in uncomplicated pregnancy.[47] TAGLN is an intracellular factor that regulates the cell surface structure of tumor endothelial marker 8, which is an integrin-like cell surface receptor (85 kDa) upregulated in tumor blood vessels.[48] TAGLN is also required for vasculogenic mimicry of BC.[29] TAGLN2, a SM22/TAGLN homolog, belongs to the actin-binding protein family[49] and is responsible for the anti-angiogenic effect induced by lovastatin on ECs. The siRNA-mediated TAGLN2 knockdown evidently enhanced EC migration and tube formation, which also mitigated lovastatin-induced inhibition of cell motility.[50]

In this study, we report for the first time that TAGLN in ECs exhibits regulatory effects on tumor vessel normalization, and thereby inhibits TB and BC progression. SAA, the agent that improves outcomes in myocardial ischemia by stabilizing the TAGLN-actin complex,[33] facilitated the normalization of tumor vessels, resulted in reduced leakage, increased perfusion, and alleviated hypoxia. Subsequently, the alleviated hypoxic condition decreases necrosis and favorably alters the tumor microenvironment to prevent tumor development (such as growth and metastasis). Reduced hypoxia levels also decrease the expression of HIF-1α, which was reported to accelerate the proliferation and invasion of tumor cells.[51]

We also determined the regulatory mechanism of TAGLN expression in ECs. Exosomes are the vesicles released by the nanoscale membrane, which act as intercellular messengers and participate in the establishment of the tumor microenvironment.[52] Tumor-derived exosomes are involved in various signaling pathways and delivery of genetic information, thereby leading to new angiogenesis and accelerating the tumor progression.[53] Several studies have been performed to examine the effects of exosome-derived miRNAs on new blood vessel formation in tumors.[54,55] miRNAs are important regulatory factors required for mRNA translation and gene expression at the post-transcriptional level and modulation of several cell functions.[56] We discovered that exosomes could transfer miR-22-3p from BC cells to ECs. Further analyses indicated that the exosomal miR-22-3p induces tumor vessel abnormalization *in vivo* and *in vitro*. miR-22-3p is frequently dysregulated in many cancer types. It is upregulated in colorectal,[57] pancreatic,[58] and prostatic cancer[59] and acts as a key regulator in cervical cancer progression.[60] Inhibition of miR-22 also suppresses the cellular proliferation and induces apoptosis in BC cells.[61] These findings imply that miR-22-3p is an oncogene. miR-22-3p can also exert tumor-suppressing effects; it is downregulated in esophageal cancer and inhibits the progression of hepatocellular carcinoma.[62] However, we could not determine whether cancer cell-derived miR-22-3p can be delivered to the ECs adjacent to cancer cells for regulating angiogenesis.

Overall, the present study demonstrated the angiogenic effect of exosome-derived miR-22-3p as well as its direct effect on TAGLN inhibition within ECs. These effects lead to tumor vessel abnormalization, thereby promoting TB and BC progression. This study provides a basis for the possible benefit of TAGLN-targeting drugs as alternative therapeutic options in cancer treatment.

MATERIALS AND METHODS

Patient samples

In this study, 128 invasive ductal carcinoma (originating from the mammary gland duct) samples were collected from the Affiliated Hospital of Jining Medical University and Tangshan Gongren Hospital. Clinicopathological data on age, tumor size, tumor grade, tumor-lymph node-metastasis (TNM) stage of the tumor, and overall survival of patients were collected. All slides were reviewed by two pathologists who defined the histological type in accordance with the World Health Organization published standards. The study was approved by the Affiliated Hospital of Jining Medical University, and all specimens were collected after obtaining informed consent from the patients. This study was performed strictly in accordance with the approved guidelines.

Immunohistochemical (IHC) assay and analysis

Paraffin slides were treated with xylene and ethanol, subjected to antigen repair, and incubated with 10% fetal bovine serum (FBS) for 20 min at room temperature. Primary antibodies were incubated overnight at 4°C. A secondary antibody labeled with horseradish peroxidase was incubated for 30 min and then stained with diaminobenzidine and hematoxylin (ZSGB-Bio, China). A staining index was used to interpret the results by analyzing both the staining intensity and the proportion of positive cells.[63]

TB assessment

Hematoxylin and eosin (H&E)-stained sections were used to assess TB, which is defined as a single cell or a cluster of fewer than five cells. After selecting a field in which TB intensity was considered maximal, the number of TBs was counted in a ×200 field, and the average of five fields was calculated.[64] Five buds were set as the cutoff for low- or high-grade budding.[65] Patients with a TB grade of <5 were defined as low budding, and those with a grade of ≥5 were defined as high budding.

MVD and MSE counting

To count the number of microvessels, we identified the vessels that were positively stained for CD34 according to the method reported by Weidner et al.[66] Subsequently, the sections were scanned at low magnification (×100) to identify the areas with the highest MVD, which were depicted as the "hot spot." Then, the microvessels were counted at high magnification (×400), whereas the MVD was determined as the mean number of three high-power fields. MSE was used to determine the degree of tumor vessel disorder.[67] To determine MSE, the images of the CD34-stained tissues obtained at ×400 magnification were captured. MSE was calculated according to the following structural entropy equation: $MSE = \Sigma[(\Delta a/a)^2 + (\Delta d/d)^2]$, where "a" denotes the microvessel area, "d" denotes the distance between adjacent microvessels, "Δa" denotes the average area from all microvessels within the interested field, and "Δd" denotes the average distance between all microvessels. The average of five fields was considered as the final MSE.

Cell culture and transfection

MCF-7 and MDA-MB-231 (MM-231) human BC cells were provided by Nanjing Keygen Cell Bank (Nanjing, China). The mouse BC cell line E0771 was obtained from Jennio Biotech (Guangdong, China). MCF-7 and MM-231 cells were maintained in RPMI 1640 medium (KeyGen, Nanjing, China), and E0771 cells were maintained in Dulbecco's modified Eagle's medium (KeyGen, Nanjing, China) containing 10% FBS (Excell, Shanghai, China). HUVECs were purchased from iCell Bioscience (Shanghai, China). The cells were cultured in EC medium (ScienCell, USA) containing basal medium, 5% FBS, 1% EC growth supplement (ECGS), and 1% penicillin/streptomycin (P/S) solution. All cells were maintained at 37°C and 5% CO_2. Subconfluent HUVECs (three to six passages) were used in the experiments. Human *TAGLN* gene open reading frame (ORF) cDNA clone expression plasmid was purchased from GeneChem (Shanghai, China). si-TAGLN was purchased from GenePharma (Shanghai, China). The lentiviral expression plasmids used to increase or decrease miR-22-3p expression were synthesized by GeneChem (Shanghai, China). Lipofectamine 2000 (Invitrogen, USA) was used for cell transfection.

Co-culture assay, exosome uptake, and exosome secretion inhibition assay

To determine the effect of the tumor microenvironment on ECs, we co-cultured BC cells and HUVECs with transwell permeable supports (JET Biofil, China; 0.4 μm), as described in a study by Cheng et al.[68] HUVECs were seeded on a 24-well plate, and BC cells were cultured in the transwell chamber. BC cells and HUVECs were co-cultured for 48 h. For exosomal uptake, HUVECs were seeded on glass in a 24-well plate overnight. The exosomes extracted from BC cells were stained with PKH26 (Thermo Scientific, USA), which were then incubated for 24 h with HUVECs. To suppress the exosome production, 10 μM GW4869 (exosome production inhibitor, Cayman Chemical, Ann Arbor, MI, USA) was used to pre-treat BC cells obtained from the established co-culture system 24 h prior to subsequent examination.

IF and cytoskeleton staining assays

Cells were inoculated into slides, followed by 4% paraformaldehyde (PFA) fixation for 20 min, 0.1% Triton X-100 treatment for 5 min, and 5% bovine serum albumin treatment for 30 min. Table S1 lists the primary antibodies used in this study. Slides were incubated with fluorescein isothiocyanate (FITC) or 5/6-tetramethyl-rhodamine isothiocyanate-labeled secondary antibody for 1 h. In the cytoskeleton staining assay, the cells were stained with rhodamine-labeled phalloidin (YESEN, China) for 15 min after fixation and blocking. The cells were then stained with 4′,6-diamidino-2-phenylindole (Sigma, USA) and observed using a confocal fluorescence microscope (Nikon, Japan). The results were quantified by analyzing the percent fluorescence and fluorescence intensity using ImageJ software.

SEM observations

Pre-cooled glutaraldehyde (2.5%) was used to fix the cells on glass for 2 h at 4°C. Subsequently, 1% osmium tetroxide (OsO_4) dissolved in 0.1 M PBS was used for post-fixing cells for 1 h. Then, the fixed cells were treated with gradient ethanol and tert-butanol dehydration. Thereafter, each sample was freeze-dried under vacuum. An SEM (JEOL 6000, JEOL, Japan) was used to observe the gold-coated cells.

Western blot analysis

Radioimmunoprecipitation assay lysis buffer was used to extract the total protein. Sodium dodecyl sulfate-polyacrylamide gel electrophoresis (SDS-PAGE) was used to separate proteins, which were then transferred to polyvinylidene fluoride (PVDF) membranes. Afterward, the membranes were blocked using 5% non-fat milk and incubated overnight with primary antibodies at 4°C. Then, the membranes were incubated with secondary antibodies and observed using an electrophoresis gel imaging system (ChemiScope 6000, CLIX, Shanghai, China).

Analysis of G-actin and F-actin

Expressions of F-actin and G-actin were determined as described previously.[28] Buffer A, consisting of 20 mM Tris-HCl (pH 7.5), 5 mM ethylene glycol tetraacetic acid (EGTA), 1% Triton X-100, and 1 mM PMSF, was used to lyse cells for 30 min on ice, followed by centrifugation for 20 min at 12,000 × *g* and 4°C. Subsequently, the supernatant (G-actin fraction) was collected, and the pellet fraction was suspended in buffer B, consisting of 10 mM Tris-HCl (pH 7.5), 1% Triton X-100, 150 mM NaCl, 2 mM EGTA, 0.1% SDS, 1 mM sodium deoxycholate, and 1 mM PMSF, for 30 min on ice, followed by centrifugation for 30 min at 12,000 × *g* and 4°C. Finally, the supernatant was collected and regarded as the F-actin fraction. Subsequently, SDS-PAGE was performed to separate proteins from the supernatants, which were then transferred to the PVDF membranes for performing western blot analysis using the anti-actin antibody (Affinity Biosciences, China). Then, the relative contents of F-actin and G-actin in the sample were examined.

Transwell assay

Cells maintained in serum-free medium were inoculated in a Matrigel (BD Biosciences, USA)-coated chamber (8 μm, JET Biofil, China) and added to each well of the 24-well plate containing a medium supplemented with 20% FBS. Then, 4% PFA was used to fix these invasive cells, 0.1% crystal violet was used to stain the cells, and the number of cells was determined after 24 h.

Tube formation assay

HUVECs (5×10^4 cells/well) were inoculated into each well of the Matrigel-coated 24-well plate. Subsequently, the tube formation was monitored and microscopic images were captured. Then, tube length and quantity and branch quantity were determined using ImageJ (National Institutes of Health, USA).

Xenograft tumor model

C57BL/6 mice were provided by Charles River Laboratories (Beijing, China). *TAGLN* gene knockout C57BL/6 mice ($Tagln^{-/-}$) were provided by Jackson Laboratory (Bar Harbor, ME, USA).[33] All of the mice were raised in a specific pathogen-free environment. All animal procedures were conducted in accordance with the protocols approved by the Institutional Animal Care and Use Committee of

Tianjin International Joint Academy of Biomedicine. The female mice (weight, 18–20 g) were adopted for establishing the xenograft model. WT and Tagln$^{-/-}$ mice were subcutaneously administered approximately 1×10^6 E0771 cells via the mid-dorsal region. The E0771 medullary breast adenocarcinoma cells were originally isolated from a spontaneous cancer in C57BL/6 mice.[69,70] The animals were divided into different groups (five mice in each group) after achieving a tumor volume of 80–100 mm^3. WT and Tagln$^{-/-}$ mice were treated with PBS or SAA (Meilunbio, China) separately. Tumor volume was calculated at intervals of 2 days by using the following formula: $V = ab^2/2$ (where "a" represents the tumor length and "b" represents the tumor width). Then, the tumor tissues were harvested for performing IHC and IF analyses. Lung tissues were also harvested for H&E staining and the lung metastasis examination. For the survival analysis, the E0771 cells were injected into the mice via the caudal vein (n = 8).

To determine whether SAA enhances the delivery of chemotherapeutics to E0771 tumors in the presence of DPP (SAA + DDP) (Meilunbio, China), we divided WT mice into four groups, namely model mice (WT), mice treated with 10 mg/kg SAA alone (WT + SAA), mice treated with 3 mg/kg DDP alone (WT + DDP), and mice treated with 3 mg/kg DDP and 10 mg/kg SAA (WT + SAA + DDP). SAA and DDP were administered intragastrically every day for 14 days.

To determine the function of exosome-derived miR-22-3p in regulating the formation of abnormal blood vessels, E0771 cells were transfected with lentivirus to knock down miR-22-3p expression (miR-22-3p KD) or to overexpress miR-22-3p (miR-22-3p OE). E0771 cells transfected with control lentivirus or miR-22-3p-overexpressed lentivirus were subcutaneously injected into the WT or Tagln$^{-/-}$ mice (1×10^6 cells/mouse, n = 5). Moreover, the exosomes obtained from control E0771 cells or miR-22-3p KD cells were isolated and injected into the E0771-bearing mice via their tail veins (10 μg/mouse) every other day for 2 weeks. Tumor diameter was measured, and the tumor tissues were collected. For the survival analysis, the E0771 cells were injected into the mice via the caudal vein.

Pimonidazole staining, vascular leakage, and perfusion analysis

A Hypoxyprobe Plus kit (Merck Millipore, USA) was used to detect hypoxic area in tumors, and the mice were injected with pimonidazole (Hypoxyprobe-1, 60 mg/kg). To evaluate vascular leakage and perfusion, the mice were treated with 100 μL of rhodamine-conjugated dextran (25 mg/mL, 70 kDa, Sigma) or 100 μL of DyLight 48-conjugated tomato lectin (1 mg/mL, Vector Laboratories). After 30 min, the mice were subjected to whole-animal perfusion in 1% PFA to remove circulating dextran or lectin before sacrifice. The tumor tissues were collected and fixed in 1% PFA and dehydrated in 20% sucrose solution overnight to prepare them for frozen sectioning and IF analyses.

Spheroid-based angiogenesis assay

HUVEC spheroids were synthesized using the hanging drop method as reported previously.[71] HUVECs were cultured in 50 μL of hanging drops containing 1×10^4 cells/drop. The HUVEC drops were hung in an inverted position on the lid of the 48-well plate for 3 days. HUVEC spheroids were embedded in Matrigel for 3 days. Images were captured using ImageJ software.

HUVEC permeability assay

HUVECs were seeded on a 0.8-μm transwell chamber coated with Matrigel and incubated with rhodamine-conjugated dextran for 1 h. The solution (100 μL) in plate wells was transferred into a 96-well plate. The Promega GloMax 96 microplate reader (Promega, USA) was used to read the fluorescence signals.

Exosome extraction from BC cells

BC cells were maintained in RPMI 1640 containing 10% exosome-depleted FBS. After 48 h, the exosomes in the supernatant were collected and purified by using a classical method described by Thery et al.[72] The morphology of exosomes was observed under a TEM (JEM 1010, JEOL, Japan). Western blot analysis was performed to determine the expression of exosomal markers (Hsp70, CD63, and TSG101).

RNA isolation and quantitative real-time PCR

TRIzol reagent (Generay Biotech, China) was used to extract the total cellular RNA. miRNA levels were quantified using a custom gene quantitative real-time PCR quantitation kit (GenePharm, China) in accordance with specific instructions and with U6 as a reference. A reverse transcription kit (TransGen, China) was used to reverse transcribe mRNA. The mRNA level was quantified using FastStart Universal SYBR Green master (ROX) (Roche, USA) in accordance with specific protocols, with glyceraldehyde 3-phosphate dehydrogenase (GAPDH) as the reference. The relative level was determined by the ΔΔCt approach. Primer designs of GAPDH and TAGLN were as follows: TAGLN, 5′-GTTCCAGACTGTTGACCTCTTT-3′ (forward), 5′-CTGCGCTTTCTTCATAAACC-3′ (reverse); and GAPDH, 5′-CTGACTTCAACAGCGACACC-3′ (forward), 5′-TGCTGTAGCCAAATTCGTTGT-3′ (reverse).

Dual-luciferase reporter gene assay

hsa-miR-22-3p-binding sites within the TAGLN sequence were predicted by referring to the TargetScan website (http://www.targetscan.org/). The dual-luciferase reporter assay was performed to determine whether TAGLN serves as the hsa-miR-33-3p direct target gene. Xbal and Nhel enzyme sites were used to digest the gene fragment of the as-prepared TAGLN 3′ UTR, which was later inserted to the pmirGLO vector. Thereafter, pmirGLO-TAGLN-mutant (MUT) and pmirGLO-TAGLN-WT (Genewiz, Shanghai, China) were synthesized and then co-transfected with hsa-miR-22-3p mimic or NC (negative control) sequence to the HUVECs. After 48 h, HUVECs were harvested and lysed. Luciferase activity was determined using a Dual-Luciferase reporter assay kit (Beyotime, China) and a luminometer .

Statistical analysis

Data are presented in the manner of mean ± standard deviation. A p value of <0.05 was considered statistically significant. For normally

distributed data, analysis of variance and a Student's test were used to assess the differences. For abnormally distributed data, differences between two or more groups were compared using the Kruskal-Wallis test or Mann-Whitney U test. The Kaplan-Meier test was used for survival analysis.

SUPPLEMENTAL INFORMATION

Supplemental Information can be found online at https://doi.org/10.1016/j.ymthe.2021.02.009.

ACKNOWLEDGMENTS

This work was supported by the National Natural Science Foundation of China (81972629, 81802945, and 81872374), the Taishan Scholars Program of Shandong Province (tsqn201909193), and by the PhD Research Foundation of Affiliated Hospital of Jining Medical University (2020-BS-001). We thank Tangshan Workers Hospital for providing the paraffin specimens.

AUTHOR CONTRIBUTIONS

Y.F. and L.W. performed the experiments and data collection and analysis. Q.X., B.Z., and Y.L. performed the cell experiments, and X.C. and Y.T. participated in the animal experiments. T.W., R.Z., L.L., and W.W. contributed to the collection of pathological data. L.L. reviewed the pathological sections. L.Y., X.Z., and L.L. performed the statistical analysis. Y.L. wrote the manuscript and designed the study. T.S. revised the manuscript.

DECLARATION OF INTERESTS

The authors declare no competing interests.

REFERENCES

1. Siegel, R.L., Miller, K.D., and Jemal, A. (2019). Cancer statistics, 2019. CA Cancer J. Clin. *69*, 7–34.
2. Hase, K., Shatney, C., Johnson, D., Trollope, M., and Vierra, M. (1993). Prognostic value of tumor "budding" in patients with colorectal cancer. Dis. Colon Rectum *36*, 627–635.
3. Kanazawa, H., Mitomi, H., Nishiyama, Y., Kishimoto, I., Fukui, N., Nakamura, T., and Watanabe, M. (2008). Tumour budding at invasive margins and outcome in colorectal cancer. Colorectal Dis. *10*, 41–47.
4. Lugli, A., Kirsch, R., Ajioka, Y., Bosman, F., Cathomas, G., Dawson, H., El Zimaity, H., Fléjou, J.F., Hansen, T.P., Hartmann, A., et al. (2017). Recommendations for reporting tumor budding in colorectal cancer based on the International Tumor Budding Consensus Conference (ITBCC) 2016. Mod. Pathol. *30*, 1299–1311.
5. Taira, T., Ishii, G., Nagai, K., Yoh, K., Takahashi, Y., Matsumura, Y., Kojima, M., Ohmatsu, H., Goto, K., Niho, S., et al. (2012). Characterization of the immunophenotype of the tumor budding and its prognostic implications in squamous cell carcinoma of the lung. Lung Cancer *76*, 423–430.
6. Yamaguchi, Y., Ishii, G., Kojima, M., Yoh, K., Otsuka, H., Otaki, Y., Aokage, K., Yanagi, S., Nagai, K., Nishiwaki, Y., and Ochiai, A. (2010). Histopathologic features of the tumor budding in adenocarcinoma of the lung: tumor budding as an index to predict the potential aggressiveness. J. Thorac. Oncol. *5*, 1361–1368.
7. Almangush, A., Salo, T., Hagström, J., and Leivo, I. (2014). Tumour budding in head and neck squamous cell carcinoma—a systematic review. Histopathology *65*, 587–594.
8. O'Connor, K., Li-Chang, H.H., Kalloger, S.E., Peixoto, R.D., Webber, D.L., Owen, D.A., Driman, D.K., Kirsch, R., Serra, S., Scudamore, C.H., et al. (2015). Tumor budding is an independent adverse prognostic factor in pancreatic ductal adenocarcinoma. Am. J. Surg. Pathol. *39*, 472–478.
9. Niwa, Y., Yamada, S., Koike, M., Kanda, M., Fujii, T., Nakayama, G., Sugimoto, H., Nomoto, S., Fujiwara, M., and Kodera, Y. (2014). Epithelial to mesenchymal transition correlates with tumor budding and predicts prognosis in esophageal squamous cell carcinoma. J. Surg. Oncol. *110*, 764–769.
10. Gujam, F.J., McMillan, D.C., Mohammed, Z.M., Edwards, J., and Going, J.J. (2015). The relationship between tumour budding, the tumour microenvironment and survival in patients with invasive ductal breast cancer. Br. J. Cancer *113*, 1066–1074.
11. Salhia, B., Trippel, M., Pfaltz, K., Cihoric, N., Grogg, A., Lädrach, C., Zlobec, I., and Tapia, C. (2015). High tumor budding stratifies breast cancer with metastatic properties. Breast Cancer Res. Treat. *150*, 363–371.
12. Liang, F., Cao, W., Wang, Y., Li, L., Zhang, G., and Wang, Z. (2013). The prognostic value of tumor budding in invasive breast cancer. Pathol. Res. Pract. *209*, 269–275.
13. De Smedt, L., Palmans, S., and Sagaert, X. (2016). Tumour budding in colorectal cancer: what do we know and what can we do? Virchows Arch. *468*, 397–408.
14. Koelzer, V.H., Zlobec, I., and Lugli, A. (2016). Tumor budding in colorectal cancer—ready for diagnostic practice? Hum. Pathol. *47*, 4–19.
15. Bronsert, P., Enderle-Ammour, K., Bader, M., Timme, S., Kuehs, M., Csanadi, A., Kayser, G., Kohler, I., Bausch, D., Hoeppner, J., et al. (2014). Cancer cell invasion and EMT marker expression: a three-dimensional study of the human cancer-host interface. J. Pathol. *234*, 410–422.
16. Masugi, Y., Yamazaki, K., Hibi, T., Aiura, K., Kitagawa, Y., and Sakamoto, M. (2010). Solitary cell infiltration is a novel indicator of poor prognosis and epithelial-mesenchymal transition in pancreatic cancer. Hum. Pathol. *41*, 1061–1068.
17. Kohler, I., Bronsert, P., Timme, S., Werner, M., Brabletz, T., Hopt, U.T., Schilling, O., Bausch, D., Keck, T., and Wellner, U.F. (2015). Detailed analysis of epithelial-mesenchymal transition and tumor budding identifies predictors of long-term survival in pancreatic ductal adenocarcinoma. J. Gastroenterol. Hepatol. *30* (*Suppl 1*), 78–84.
18. Wang, C., Huang, H., Huang, Z., Wang, A., Chen, X., Huang, L., Zhou, X., and Liu, X. (2011). Tumor budding correlates with poor prognosis and epithelial-mesenchymal transition in tongue squamous cell carcinoma. J. Oral Pathol. Med. *40*, 545–551.
19. Mitrovic, B., Schaeffer, D.F., Riddell, R.H., and Kirsch, R. (2012). Tumor budding in colorectal carcinoma: time to take notice. Mod. Pathol. *25*, 1315–1325.
20. Kalluri, R., and Weinberg, R.A. (2009). The basics of epithelial-mesenchymal transition. J. Clin. Invest. *119*, 1420–1428.
21. Grigore, A.D., Jolly, M.K., Jia, D., Farach-Carson, M.C., and Levine, H. (2016). Tumor budding: the name is EMT. Partial EMT. J. Clin. Med. *5*, 51.
22. Ferrara, N., and Kerbel, R.S. (2005). Angiogenesis as a therapeutic target. Nature *438*, 967–974.
23. Ribatti, D., Nico, B., Crivellato, E., and Vacca, A. (2007). The structure of the vascular network of tumors. Cancer Lett. *248*, 18–23.
24. Carmeliet, P., and Jain, R.K. (2011). Principles and mechanisms of vessel normalization for cancer and other angiogenic diseases. Nat. Rev. Drug Discov. *10*, 417–427.
25. Gerstner, E.R., Duda, D.G., di Tomaso, E., Ryg, P.A., Loeffler, J.S., Sorensen, A.G., Ivy, P., Jain, R.K., and Batchelor, T.T. (2009). VEGF inhibitors in the treatment of cerebral edema in patients with brain cancer. Nat. Rev. Clin. Oncol. *6*, 229–236.
26. Sung, Y.C., Jin, P.R., Chu, L.A., Hsu, F.F., Wang, M.R., Chang, C.C., Chiou, S.J., Qiu, J.T., Gao, D.Y., Lin, C.C., et al. (2019). Delivery of nitric oxide with a nanocarrier promotes tumour vessel normalization and potentiates anti-cancer therapies. Nat. Nanotechnol. *14*, 1160–1169.
27. Camoretti-Mercado, B., Forsythe, S.M., LeBeau, M.M., Espinosa, R., 3rd, Vieira, J.E., Halayko, A.J., Willadsen, S., Kurtz, B., Ober, C., Evans, G.A., et al. (1998). Expression and cytogenetic localization of the human SM22 gene (TAGLN). Genomics *49*, 452–457.
28. Han, M., Dong, L.H., Zheng, B., Shi, J.H., Wen, J.K., and Cheng, Y. (2009). Smooth muscle 22 alpha maintains the differentiated phenotype of vascular smooth muscle cells by inducing filamentous actin bundling. Life Sci. *84*, 394–401.
29. Aikins, A.R., Kim, M., Raymundo, B., and Kim, C.W. (2017). Downregulation of transgelin blocks interleukin-8 utilization and suppresses vasculogenic mimicry in breast cancer cells. Exp. Biol. Med. (Maywood) *242*, 573–583.

30. Théry, C., Zitvogel, L., and Amigorena, S. (2002). Exosomes: composition, biogenesis and function. Nat. Rev. Immunol. *2*, 569–579.

31. Kalluri, R. (2016). The biology and function of exosomes in cancer. J. Clin. Invest. *126*, 1208–1215.

32. Pakravan, K., Babashah, S., Sadeghizadeh, M., Mowla, S.J., Mossahebi-Mohammadi, M., Ataei, F., Dana, N., and Javan, M. (2017). MicroRNA-100 shuttled by mesenchymal stem cell-derived exosomes suppresses in vitro angiogenesis through modulating the mTOR/HIF-1α/VEGF signaling axis in breast cancer cells. Cell Oncol. (Dordr.) *40*, 457–470.

33. Zhong, W., Sun, B., Gao, W., Qin, Y., Zhang, H., Huai, L., Tang, Y., Liang, Y., He, L., Zhang, X., et al. (2018). Salvianolic acid A targeting the transgelin-actin complex to enhance vasoconstriction. EBioMedicine *37*, 246–258.

34. Zhou, B., Zong, S., Zhong, W., Tian, Y., Wang, L., Zhang, Q., Zhang, R., Li, L., Wang, W., Zhao, J., et al. (2020). Interaction between laminin-5γ2 and integrin β1 promotes the tumor budding of colorectal cancer via the activation of Yes-associated proteins. Oncogene *39*, 1527–1542.

35. Yang, X.Y., Yao, J.H., Cheng, L., Wei, D.W., Xue, J.L., and Lu, D.R. (2003). Molecular cloning and expression of a smooth muscle-specific gene SM22α in zebrafish. Biochem. Biophys. Res. Commun. *312*, 741–746.

36. Maleszewska, M., Gjaltema, R.A., Krenning, G., and Harmsen, M.C. (2015). Enhancer of zeste homolog-2 (EZH2) methyltransferase regulates transgelin/smooth muscle-22α expression in endothelial cells in response to interleukin-1β and transforming growth factor-β2. Cell. Signal. *27*, 1589–1596.

37. Aslan, C., Maralbashi, S., Salari, F., Kahroba, H., Sigaroodi, F., Kazemi, T., and Kharaziha, P. (2019). Tumor-derived exosomes: implication in angiogenesis and antiangiogenesis cancer therapy. J. Cell. Physiol. *234*, 16885–16903.

38. Ludwig, N., Yerneni, S.S., Razzo, B.M., and Whiteside, T.L. (2018). Exosomes from HNSCC promote angiogenesis through reprogramming of endothelial cells. Mol. Cancer Res. *16*, 1798–1808.

39. Hsu, Y.L., Hung, J.Y., Chang, W.A., Lin, Y.S., Pan, Y.C., Tsai, P.H., Wu, C.Y., and Kuo, P.L. (2017). Hypoxic lung cancer-secreted exosomal miR-23a increased angiogenesis and vascular permeability by targeting prolyl hydroxylase and tight junction protein ZO-1. Oncogene *36*, 4929–4942.

40. Wu, X.G., Zhou, C.F., Zhang, Y.M., Yan, R.M., Wei, W.F., Chen, X.J., Yi, H.Y., Liang, L.J., Fan, L.S., Liang, L., et al. (2019). Cancer-derived exosomal miR-221-3p promotes angiogenesis by targeting THBS2 in cervical squamous cell carcinoma. Angiogenesis *22*, 397–410.

41. Bergers, G., and Hanahan, D. (2008). Modes of resistance to anti-angiogenic therapy. Nat. Rev. Cancer *8*, 592–603.

42. Jain, R.K. (2014). Antiangiogenesis strategies revisited: from starving tumors to alleviating hypoxia. Cancer Cell *26*, 605–622.

43. Shields, J.M., Rogers-Graham, K., and Der, C.J. (2002). Loss of transgelin in breast and colon tumors and in RIE-1 cells by Ras deregulation of gene expression through Raf-independent pathways. J. Biol. Chem. *277*, 9790–9799.

44. Lee, E.K., Han, G.Y., Park, H.W., Song, Y.J., and Kim, C.W. (2010). Transgelin promotes migration and invasion of cancer stem cells. J. Proteome Res. *9*, 5108–5117.

45. Rao, D., Kimler, B.F., Nothnick, W.B., Davis, M.K., Fan, F., and Tawfik, O. (2015). Transgelin: a potentially useful diagnostic marker differentially expressed in triple-negative and non-triple-negative breast cancers. Hum. Pathol. *46*, 876–883.

46. Zhou, H.M., Fang, Y.Y., Weinberger, P.M., Ding, L.L., Cowell, J.K., Hudson, F.Z., Ren, M., Lee, J.R., Chen, Q.K., Su, H., et al. (2016). Transgelin increases metastatic potential of colorectal cancer cells in vivo and alters expression of genes involved in cell motility. BMC Cancer *16*, 55.

47. Varberg, K.M., Garretson, R.O., Blue, E.K., Chu, C., Gohn, C.R., Tu, W., and Haneline, L.S. (2018). Transgelin induces dysfunction of fetal endothelial colony-forming cells from gestational diabetic pregnancies. Am. J. Physiol. Cell Physiol. *315*, C502–C515.

48. St Croix, B., Rago, C., Velculescu, V., Traverso, G., Romans, K.E., Montgomery, E., Lal, A., Riggins, G.J., Lengauer, C., Vogelstein, B., and Kinzler, K.W. (2000). Genes expressed in human tumor endothelium. Science *289*, 1197–1202.

49. Zhang, J.C., Helmke, B.P., Shum, A., Du, K., Yu, W.W., Lu, M.M., Davies, P.F., and Parmacek, M.S. (2002). SM22β encodes a lineage-restricted cytoskeletal protein with a unique developmentally regulated pattern of expression. Mech. Dev. *115*, 161–166.

50. Xiao, Y., Li, Y., Han, J., Pan, Y., Tie, L., and Li, X. (2012). Transgelin 2 participates in lovastatin-induced anti-angiogenic effects in endothelial cells through a phosphorylated myosin light chain-related mechanism. PLoS ONE *7*, e46510.

51. Li, A.G., Murphy, E.C., Culhane, A.C., Powell, E., Wang, H., Bronson, R.T., Von, T., Giobbie-Hurder, A., Gelman, R.S., Briggs, K.J., et al. (2018). BRCA1-IRIS promotes human tumor progression through PTEN blockade and HIF-1α activation. Proc. Natl. Acad. Sci. USA *115*, E9600–E9609.

52. Milane, L., Singh, A., Mattheolabakis, G., Suresh, M., and Amiji, M.M. (2015). Exosome mediated communication within the tumor microenvironment. J. Control. Release *219*, 278–294.

53. Komaki, M., Numata, Y., Morioka, C., Honda, I., Tooi, M., Yokoyama, N., Ayame, H., Iwasaki, K., Taki, A., Oshima, N., and Morita, I. (2017). Exosomes of human placenta-derived mesenchymal stem cells stimulate angiogenesis. Stem Cell Res. Ther. *8*, 219.

54. Zhang, L., Wu, X., Luo, C., Chen, X., Yang, L., Tao, J., and Shi, J. (2013). The 786-0 renal cancer cell-derived exosomes promote angiogenesis by downregulating the expression of hepatocyte cell adhesion molecule. Mol. Med. Rep. *8*, 272–276.

55. He, L., Zhu, W., Chen, Q., Yuan, Y., Wang, Y., Wang, J., and Wu, X. (2019). Ovarian cancer cell-secreted exosomal miR-205 promotes metastasis by inducing angiogenesis. Theranostics *9*, 8206–8220.

56. Ambros, V. (2004). The functions of animal microRNAs. Nature *431*, 350–355.

57. Schee, K., Lorenz, S., Worren, M.M., Günther, C.C., Holden, M., Hovig, E., Fodstad, O., Meza-Zepeda, L.A., and Flatmark, K. (2013). Deep sequencing the microRNA transcriptome in colorectal cancer. PLoS ONE *8*, e66165.

58. Hussein, N.A., Kholy, Z.A., Anwar, M.M., Ahmad, M.A., and Ahmad, S.M. (2017). Plasma miR-22-3p, miR-642b-3p and miR-885-5p as diagnostic biomarkers for pancreatic cancer. J. Cancer Res. Clin. Oncol. *143*, 83–93.

59. Knyazev, E.N., Samatov, T.R., Fomicheva, K.A., Nyushko, K.M., Alekseev, B.Y., and Shkurnikov, M.Y. (2016). MicroRNA hsa-miR-4674 in hemolysis-free blood plasma is associated with distant metastases of prostatic cancer. Bull. Exp. Biol. Med. *161*, 112–115.

60. Lv, K.T., Liu, Z., Feng, J., Zhao, W., Hao, T., Ding, W.Y., Chu, J.P., and Gao, L.J. (2018). miR-22-3p regulates cell proliferation and inhibits cell apoptosis through targeting the eIF4EBP3 gene in human cervical squamous carcinoma cells. Int. J. Med. Sci. *15*, 142–152.

61. Wang, B., Li, D., Filkowski, J., Rodriguez-Juarez, R., Storozynsky, Q., Malach, M., Carpenter, E., and Kovalchuk, O. (2018). A dual role of miR-22 modulated by RelA/p65 in resensitizing fulvestrant-resistant breast cancer cells to fulvestrant by targeting FOXP1 and HDAC4 and constitutive acetylation of p53 at Lys382. Oncogenesis *7*, 54.

62. Chen, J., Wu, F.X., Luo, H.L., Liu, J.J., Luo, T., Bai, T., Li, L.Q., and Fan, X.H. (2016). Berberine upregulates miR-22-3p to suppress hepatocellular carcinoma cell proliferation by targeting Sp1. Am. J. Transl. Res. *8*, 4932–4941.

63. Liu, Y., Ji, R., Li, J., Gu, Q., Zhao, X., Sun, T., Wang, J., Li, J., Du, Q., and Sun, B. (2010). Correlation effect of EGFR and CXCR4 and CCR7 chemokine receptors in predicting breast cancer metastasis and prognosis. J. Exp. Clin. Cancer Res. *29*, 16.

64. Ueno, H., Murphy, J., Jass, J.R., Mochizuki, H., and Talbot, I.C. (2002). Tumour "budding" as an index to estimate the potential of aggressiveness in rectal cancer. Histopathology *40*, 127–132.

65. Voutsadakis, I.A. (2018). Prognostic role of tumor budding in breast cancer. World J. Exp. Med. *8*, 12–17.

66. Weidner, N., Semple, J.P., Welch, W.R., and Folkman, J. (1991). Tumor angiogenesis and metastasis—correlation in invasive breast carcinoma. N. Engl. J. Med. *324*, 1–8.

67. Vidal, S., Horvath, E., Kovacs, K., Lloyd, R.V., and Scheithauer, B.W. (2003). Microvascular structural entropy: a novel approach to assess angiogenesis in pituitary tumors. Endocr. Pathol. *14*, 239–247.

68. Cheng, H.W., Chen, Y.F., Wong, J.M., Weng, C.W., Chen, H.Y., Yu, S.L., Chen, H.W., Yuan, A., and Chen, J.J. (2017). Cancer cells increase endothelial cell tube formation

and survival by activating the PI3K/Akt signalling pathway. J. Exp. Clin. Cancer Res. *36*, 27.

69. Sugiura, K., Stock, C.C., and Sugiura, M. (1952). Studies in a tumor spectrum. II. The growth of a variety of mouse and rat tumors. Cancer *5*, 979–991.

70. Dunham, L.J., and Stewart, H.L. (1953). A survey of transplantable and transmissible animal tumors. J. Natl. Cancer Inst. *13*, 1299–1377.

71. Pfisterer, L., and Korff, T. (2016). Spheroid-based in vitro angiogenesis model. Methods Mol. Biol *1430*, 167–177.

72. Thery, C., Amigorena, S., Raposo, G., and Clayton, A. (2006). Isolation and characterization of exosomes from cell culture supernatants and biological fluids. Curr. Protoc. Cell Biol. Chapter 3:Unit 3.22.

YMTHE, Volume *29*

Supplemental Information

Tumor cell-secreted exosomal miR-22-3p inhibits transgelin and induces vascular abnormalization to promote tumor budding

Yaju Feng, Lumeng Wang, Ting Wang, Ying Li, Qingqing Xun, Renya Zhang, Lin Liu, Lei Li, Wei Wang, Yixuan Tian, Lili Yang, Xiao Zhi, Bijiao Zhou, Xin Chen, Tao Sun, and Yanrong Liu

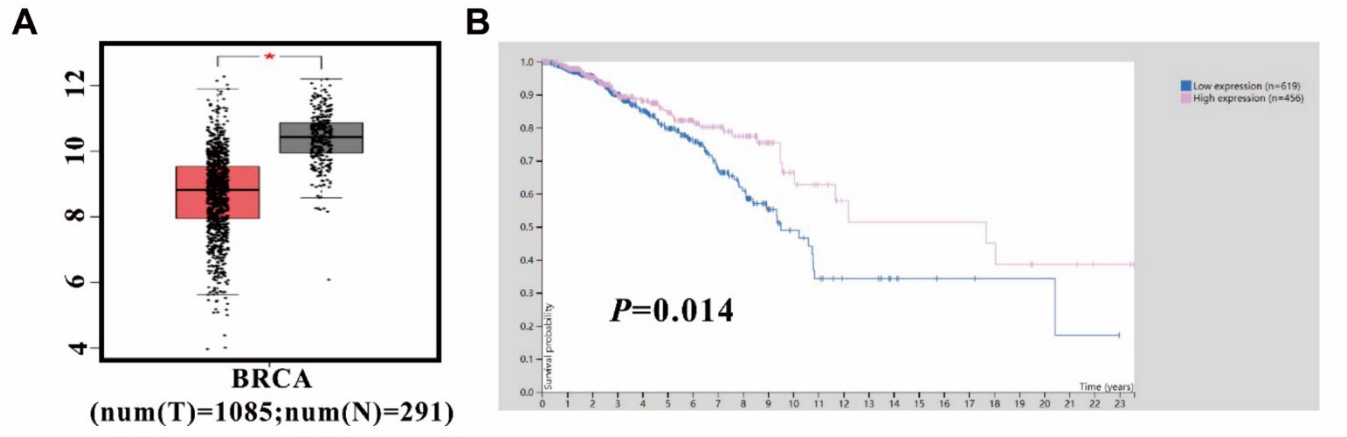

Figure S1. Transgelin expression in BRCA tissues was examined via TCGA analysis. A. Transgelin expression in BRCA tissues was lower than that in normal breast tissues. B. Patients with BRCA with high Transgelin expression have longer survival.

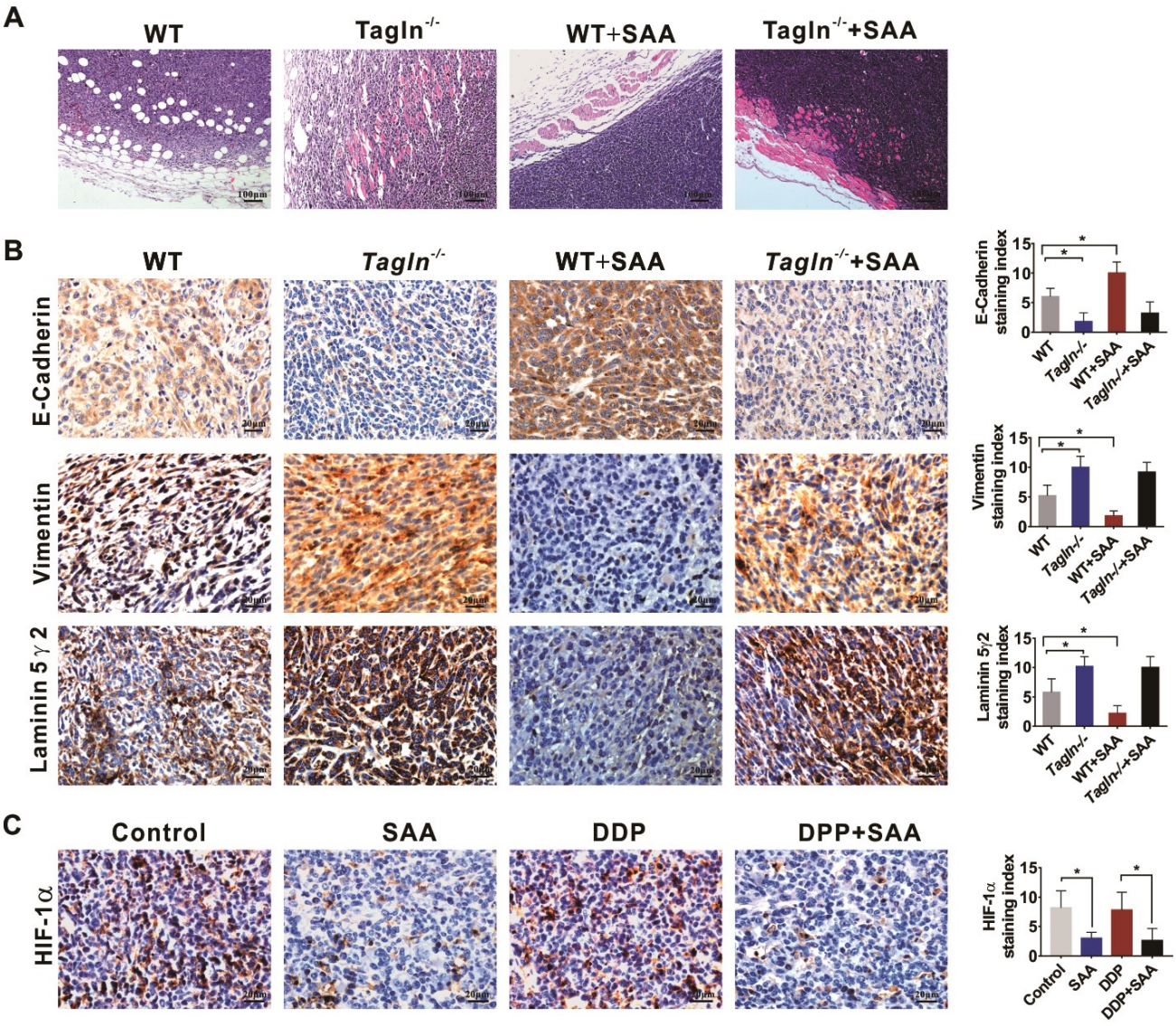

Figure S2. The invasion areas and expression of EMT related markers in E0771 tumors in WT and Tagln-/- mice. A. Hematoxylin and eosin staining of the transplanted tumor tissues showing the invasion of neighboring tissues. B. Expression levels of E-cadherin, vimentin, and laminin 5γ2 in the transplanted tumor tissues of different groups detected using IHC assays. C. The expression of HIF-1α in the transplanted tumor tissues detected by IHC staining.

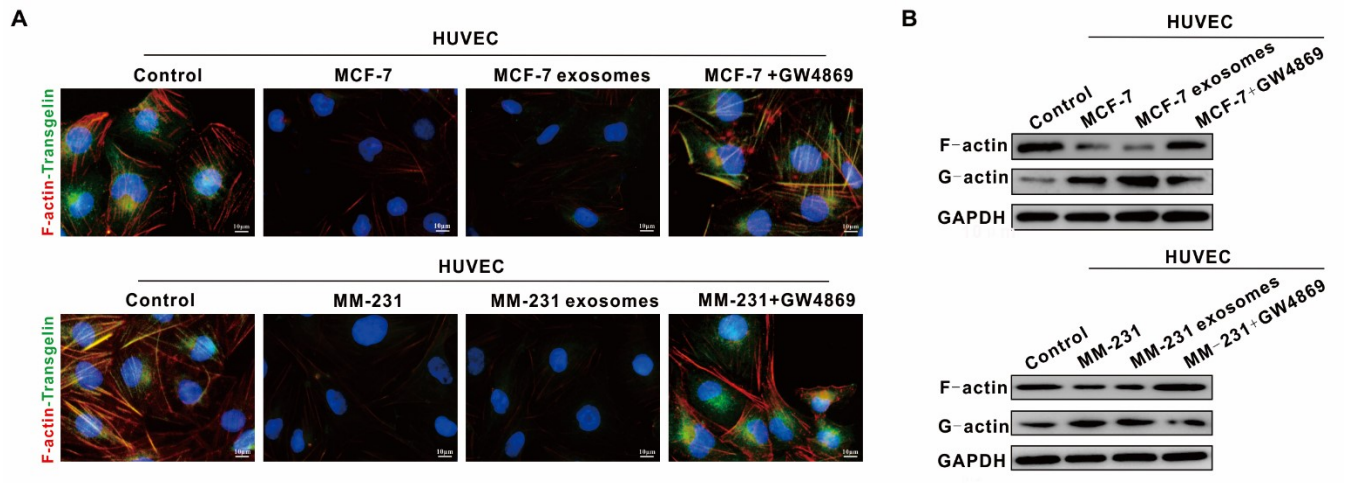

Figure S3. The effects of BC derived exosomes on the expression of Transgelin and F-actin. A. IF staining was performed to analyze the F-actin cytoskeleton and Transgelin. B. F-actin and G-actin levels in HUVECs with different treatments were detected through western blotting.

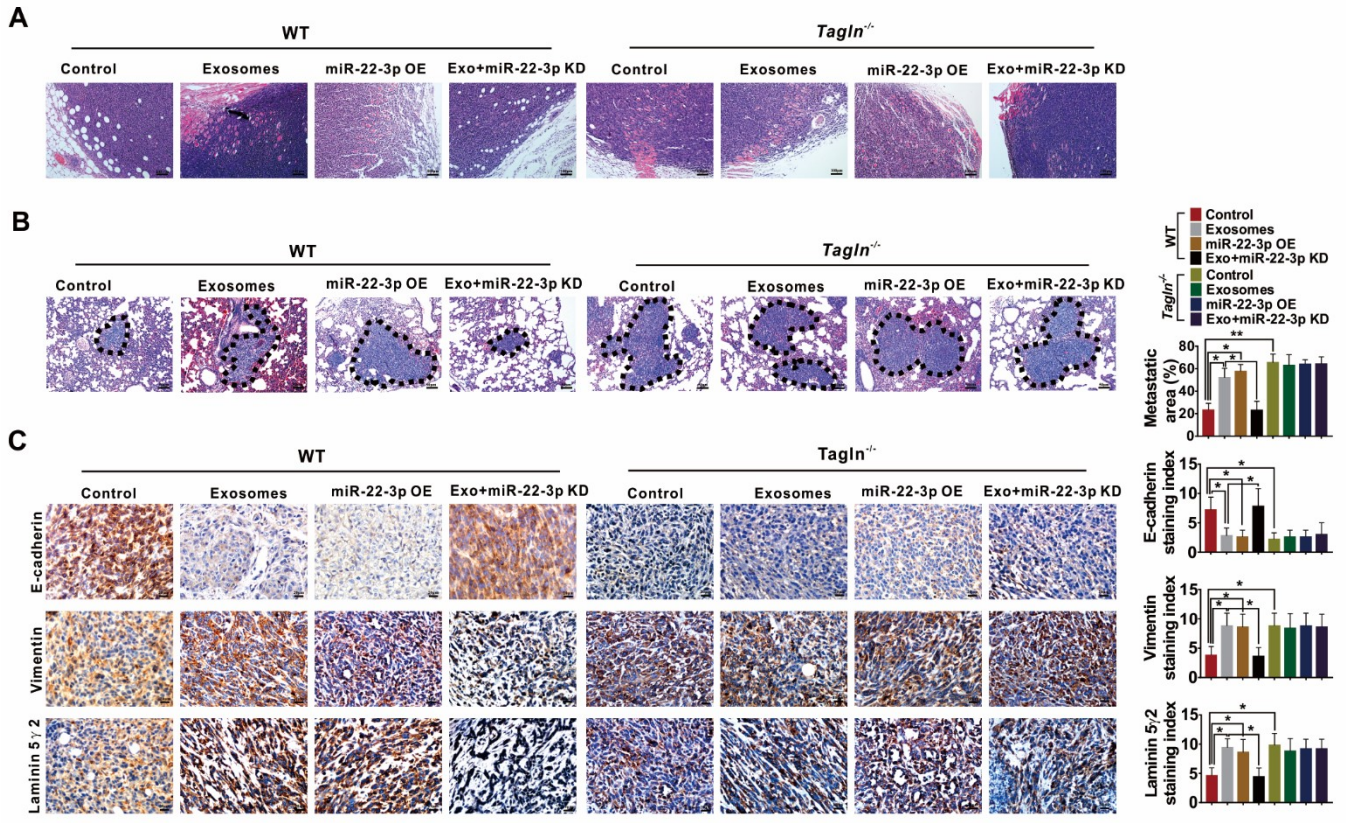

Figure S4. Exosomal miR-22-3p enhanced invasion, metastasis and expression of EMT markers of WT tumors but did not affect *Tagln*$^{-/-}$ tumors. A. Representative images of the invasion areas in H&E-stained E0771 tumors from WT and *Tagln*$^{-/-}$ mice. B. Lung metastasis areas were examined in H&E- stained tissue sections. The dotted line demarcates the metastasis areas. C. Expression levels of E-cadherin, vimentin, and laminin 5 γ 2 in the transplanted tumor tissues of different groups detected using IHC assays.

Table S1. Primary Antibodies used for WB, IF and IHC

Antibody	Type	Company	Catalogue Number
E-cadherin	Rabbit polyclonal	Affinity	AF0131
VE-cadherin	Rabbit polyclonal	Abcam	ab33168
Vimentin	Rabbit polyclonal	Affinity	AF7013
GAPDH	Mouse monoclonal	Affinity	AF7021
Laminin 5 γ2	Mouse polyclonal	Merck Millipore	sc-13587
CD34	Mouse monoclonal	Invitrogen	MA1-19229
PDGFR β	Rabbit polyclonal	Affinity	AF6133
COL IV	Mouse monoclonal	Abcam	ab86042
Transgelin	Rabbit polyclonal	Abcam	ab155272
CD63	Rabbit polyclonal	Affinity	DF2305
TSG101	Rabbit polyclonal	Affinity	DF8427
Hsp70	Rabbit polyclonal	Affinity	AF5466
β-actin	Mouse monoclonal	Affinity	T0022